AN ANALYTICAL APPROACH FOR MODELLING UNMANNED AERIAL VEHICLES AND BASE STATION INTERACTION FOR DISASTER RECOVERY SCENARIOS

A THESIS SUBMITTED TO
THE BOARD OF GRADUATE PROGRAMS
OF
MIDDLE EAST TECHNICAL UNIVERSITY, NORTHERN CYPRUS CAMPUS

BY
EUGENE OWILLA

IN PARTIAL FULFILLMENT OF THE REQUIREMENTS
FOR
THE DEGREE OF MASTER OF SCIENCE
IN COMPUTER ENGINEERING

AUGUST 2022

Approval of the Board of Graduate Programs

Prof. Dr. Cumali Sabah
Chairperson

I certify that this thesis satisfies all the requirements as a thesis for the degree of Master of Science.

Assoc. Prof. Dr. Enver Ever
Program Coordinator

This is to certify that we have read this thesis and that in our opinion it is fully adequate, in scope and quality, as a thesis for the degree of Master of Science .

Assoc. Prof. Dr. Enver Ever
Supervisor

Examining Committee Members

Assoc. Prof. Dr. Yeliz Yeşilada CNG / METU NCC

Assoc. Prof. Dr. Enver Ever CNG / METU NCC

Assoc. Prof. Dr. Eser Gemikonaklı CNG / Girne University

I hereby declare that all information in this document has been obtained and presented in accordance with academic rules and ethical conduct. I also declare that, as required by these rules and conduct, I have fully cited and referenced all material and results that are not original to this work.

Name, Last name: Eugene, Owilla

Signature:

ABSTRACT

AN ANALYTICAL APPROACH FOR MODELLING UNMANNED AERIAL VEHICLES AND BASE STATION INTERACTION FOR DISASTER RECOVERY SCENARIOS

Owilla, Eugene

Master of Science, Computer Engineering Program

Supervisor: Assoc. Prof. Dr. Enver Ever

August 2022, 79 pages

Unmanned Aerial Vehicles (UAVs) are an emerging technology with the potential to be used in various sectors for a wide array of applications and services. In wireless networking, UAVs are a vital part of supplementary infrastructure aimed at improving coverage principally during public safety crises. Due to their relatively low cost and scalability of use, there has been a mushrooming focus into the roles that UAVs can play in ameliorating service provided to stranded ground devices. Following a public safety crisis that impacts key communication infrastructure, large areas may lose cellular coverage. This prompts the need for the employment of D2D communication frameworks as a complement. In this way, the region of interest remains active during recovery operations. In such critical conditions, timely response and network connectivity are important factors for reliable communication. For instance, D2D features facilitate direct communication between first responders and rescue teams. This study focuses on the mathematics of UAVs in the context of disaster recovery. Particularly, we aim to model a queuing framework comprising UAVs as mobile relay nodes between the stranded user devices and neighbouring operational base stations. We present an iterative solution with a novel method for generating initial conditions for the two-stage queuing model and evaluate it with a custom discrete-event simulation for very large queue sizes and further analyse the impact of mobile relaying on mean queue length, throughput, and response time.

Keywords: UAV relay nodes, Disaster recovery, Two-stage queuing, Iterative solution

ÖZ

AFET KURTARMA SENARYOLARI KAPSAMINDA İNSANSIZ HAVA ARAÇLARI VE BAZ İSTASYONU ETKİLEŞİMİ İÇİN ANALİTİK MODELLEME YAKLAŞIMI

Owilla, Eugene
Yüksek Lisans, Bilgisayar Mühendisliği Programı
Tez Yöneticisi: Doç. Dr. Enver Ever

Ağustos 2022, 79 sayfa

İnsansız Hava Araçları (İHA'lar) çeşitli sektörlerde çok çeşitli uygulama ve hizmetler için kullanılabilirler. Kablosuz iletişim alanında, İHA lar felaket durumlarında oluşturulabilecek kapsama alanını destekleyici altyapının önemli parçalarıdırlar. Nispeten düşük maliyetleri ve kullanım ölçeklenebilirlikleri sebebi ile mevcut altyapılara destekleyici roller oynayabilirler. İletişim altyapısını etkilemesi muhtemel felaket durumlarında hücresel ağlar olumsuz olarak etkilenebilir ve cihazdan cihaza (D2D) iletişim yöntemleri gereksinimi doğabilir. Bu şekilde ilgili bölgenin en azından bir kısmı arama kurtarma faliyetlerini destekleyebilecek şekilde aktif iletişimin bir parçası olarak kullanılabilir. Bu gibi kritik şartlar altında zamanında müdahale ve ağ bağlantıları güvenli iletişim için önemli faktörlerdir. Örneğin, D2D özellikleri kapsama alanı dışında ilk yardım ve kurtarma ekipleri arasında doğrudan iletişim için kullanılabilirler. Bu çalışma felaket kurtarma bağlamında İHA'ların matematiksel modellemesine odaklanmaktadır. Özellikle İHA'ların yardım bekleyen kullanıcılar ile çalışır durumdaki baz istasyonları arasında röle düğümleri olarak kullanıldığı sistemler kuyruk teorisi çerçevesinde modellenmişlerdir. İki aşamalı kuyruk modelleri için özgün yinelemeli bir matematiksel çözüm yöntemi önerilmiş ve önereilen çözüm simülasyon metodu ile değerlendirilmiştir. Büyük kuyruk kapasitelerine sahip sistemler üzerinde farklı system parametrelerinin ortalama kuyruk uzunluğu, verim ve tepki süresi üzerindeki etkileri analiz edilmiştir.

Anahtar Kelimeler: İHA röle düğümleri, Afet kurtarma, İki aşamalı kuyruk, Yinelemeli çözüm

ACKNOWLEDGMENTS

The author wishes to express his deepest gratitude to his supervisor Assoc. Prof. Dr. Enver Ever for his guidance, advice, criticism, encouragement, and insight throughout the research.

The author would also like to thank Assoc. Prof. Dr. Yeliz Yeşilada as well as Assoc. Prof. Dr. Eser Gemikonaklı for their support, suggestions and comments.

TABLE OF CONTENTS

LIST OF TABLES

TABLES

LIST OF FIGURES

FIGURES

LIST OF ABBREVIATIONS

ABBREVIATIONS

UAVs	Unmanned Aerial Vehicles
UAV-RNs	Unmanned Aerial Vehicle - Relay Nodes
BSs	Base Stations
CH	Cluster Head
MQL	Mean Queue Length
RT	Response Time

CHAPTER 1

INTRODUCTION

Continuous coverage is the most important feature of any disaster recovery communication infrastructure. This is attributed to the myriad of minute factors affecting both stranded individuals on the ground and search and rescue teams, that are ever-changing within a split-second. Following this, the necessity arises for uninterrupted network coverage strategies in this context. Most notably, the use of on-ground devices [3] and UAVs [1] come to mind. The latter being our focus, we further cite the mobile nature of this solution to improve resource management and provide more control to search and rescue authorities, as will be highlighted later.

Localised public safety crises come in the form of man-made actions such as terror attacks or naturally via earthquakes. When a public safety crisis occurs, man-made or natural, base stations that are vital to provision of wireless network coverage are likely to get compromised either via physical damage to them or resulting power outages. Existing frameworks employed to alleviate network needs involving the use of Unmanned Aerial Vehicles (UAVs) could be criticised with regard to their optimisation of available resources (most notably, energy and temporal) or are at the very least still contingent on uninterrupted functioning of ground devices for their success.

The aforementioned circumstances cause significant hindrances to search and rescue operations during which speed and precision is of utmost importance. Tangentially, search and rescue operations require targeted information regarding the whereabouts of the persons within the disaster recovery environment. In such a situation, it is necessary to employ a framework that involves unifying infrastructure with as little overhead as possible.

For this reason, mobile devices are a suitable candidate in tracking the movement and

location of stranded individuals in the inactive cell. Additionally, we need to connect the stranded devices on the ground to the operational base stations in neighboring cells. The latter can be accomplished via a number of ways.

In light of this, several strategies have been explored both in academia and industry to come up with viable solutions. Recent research has pointed to the use of UAVs to outmanoeuvre the aforementioned obstacles.

In [4], Erdelj and Natalizio illustrated the disaster management applications of UAV networks and discussed some open research issues. A UAV flight path was optimized by Christy et al. for device-to-device (D2D) communication in disasters in [5] with the purpose of satisfying energy constraints. The implementation of relaying with multiple UAVs with multi-hop links and dual-hop links was explored by Chen et al. in [6]. Moreover, optimal hovering positions for UAVs were discussed at length. It would also serve the reader well to note that in the aforementioned schemes, the insight given is heavily on hovering/relatively stationary UAVs that are deployed as substitute BSs and/or relay nodes. Two typical multi-UAV relaying schemes of a single multi-hop link and multiple dual-hop links were studied by Chen et al. in [6], in which the optimal hovering positions were derived.

One popular UAV-assisted method of alleviating wireless networking needs in a disaster recovery situation is employing the use of UAVs as substitute base stations. In this case the UAV hovers above the stranded cell and provides cellular coverage for data and voice packets to the mobile devices on the ground. In such scenarios, the UAV deployed is not mobile and the concept does not provide for incorporating the mobility related factors into the models presented.

In some cases, it is possible to employ an integrated schema that involves the use of both UAVs and ground cluster heads. Such an implementation would take the form shown in Figure 1.1 below gleaned from [1].

The study in [1] explores two scenarios. Similar to the previously mentioned cases, the first scenario proposed involves the use of a single stationary UAV deployed in the stranded cell to provide coverage. The deployed UAV has to link to an emergency

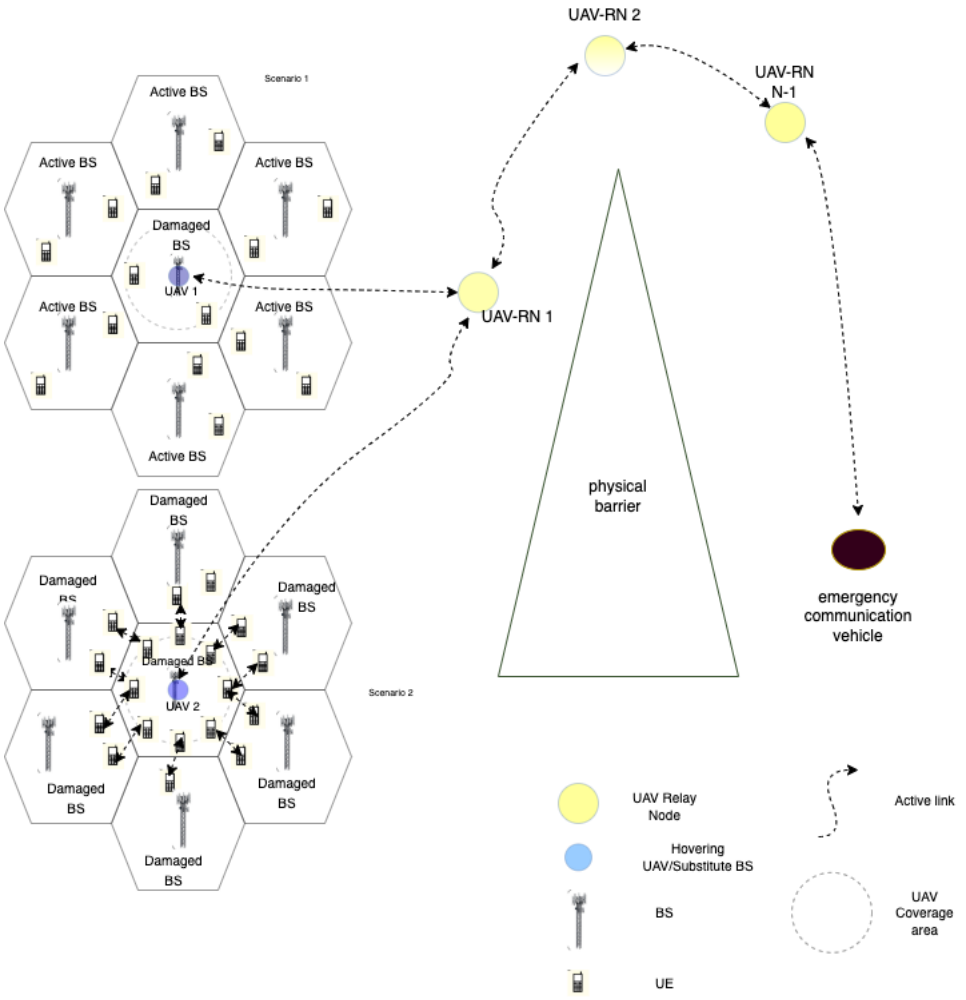

Figure 1.1 Integrating ground cluster heads with UAVs [1].

communication vehicle located quite some distance away but this is solved by the use of more UAV relay nodes (denoted as "UAV-RN 1, UAV-RN 2, ...") between the source [the deployed UAV in the stranded cell] and the sink [the emergency communication vehicle]. It would be prudent to note that in this scenario, we still have the neighbouring cells with fully operational base stations. Such a localised disaster area is the focus of our study as well.

The second scenario (denoted "Scenario 2") proposed in this study entails a ground cluster (or several clusters) communicating with an elected cluster head, which then communicates with a deployed UAV hovering above the stranded cell. The hovering UAV in turn has links to one or more relay nodes (other UAVs) positioned between it

and an emergency communication vehicle located outside the disaster recovery area. The emergency communication is a more mobile makeshift base station and thus it acts as the gateway between the stranded cell and the operational stations outside the disaster area. It is important to note that the UAVs deployed in this case are stationary, hence the need for multiple UAVs used as relay nodes.

It is the sentiment that this study provides a good preamble for our study (especially the first scenario discussed with neighboring operational base stations) as we will see in the succeeding section (2.1). This schema depicted above is also predominantly used to circumvent physical barriers such as shown in Figure 1.1 as well as servicing disaster areas of very large geographic size and focuses on provision of prolonged voice and data.

Nonetheless, the network provision enhancement approach/es that depend/s on ground devices within the packet delivery chain is susceptible to a few pitfalls:

1. **Election algorithms**: The existing standards such as explored in [7], predominantly used for Wireless Sensory Networks (WSNs), for electing cluster heads are error prone or at the very least, are predicated on assumptions that would otherwise not hold in a disaster recovery environment. For instance, in the proposed energy-efficient election strategy in [7], the assertion that the position of the candidate devices ought to be fixed would not be possible to adhere to. Seeing as providing a solution for countering this is not the focus of our study, we shall proceed under the assumption that the deployed UAV-RNs are all of equal capabilities thus negating the need for an election algorithm.

2. **Volatility of the disaster environment**: Piggybacking on the previous point, ground cluster heads are still mobile devices that are most likely on the person. This means that the topology of ground devices is ever changing. This means that they could move away from the area of coverage causing packet loss. Switching time required creates an overhead and interruption of data flow that is detrimental to search and rescue operations. In contrast, the proposed system model provides the deployment authority with better control or at the very least, knowledge about the topology of the UAV-RNs for optimum throughput.

Moreover, some public safety crises may create an environment (physical barriers between devices, thick smoke, extreme weather conditions, etc) that cannot facilitate the weaker (in comparison to a dedicated signal generated by a UAV relay node) nature of signals generated by ground cluster heads. In comparison, the proposed model ensures that the deployment authorities are aware of which areas of the disaster recovery site require what resources. If a region is experiencing weaker coverage, it is much easier and faster to deploy additional UAV-RNs or decrease the velocity and altitude of the deployed UAV-RN to improve coverage.

3. **Energy concerns**: A critique of this can be delivered in the form of:

   - The energy consumption requirements of the candidate/elected cluster heads is not known to the authority deploying the emergency network. To this effect, electing a device (or indeed successive election of cluster heads) with unreliable battery life would severely hamper search and rescue operations because of the timing overhead required to switch each time the active cluster head runs out of power.
   - In the event of a strategy that does result in the selection of the ground device with the best energy consumption as the cluster head, this device is still likely to have a lower battery life than a UAV relay node. Furthermore, if the search and rescue operations run beyond the battery lives of all possible cluster heads in the localised disaster area, we may end up with a scenario where the devices on the ground can no longer be located since they will be off. On the other hand, a pure UAV-based schema such as the one we propose ensures the control of the UAV's energy consumption levels lies with the deployment authority.

4. **Security**: In the event that the public safety crisis is of man-made origin, signals generated by ground devices acting as cluster heads are more susceptible to being compromised by malicious parties.

5. **Interoperability**: The use of ground devices to alleviate coverage needs requires knowledge of the interoperability features of the candidate cluster heads.

Most strategies depend random selection of cluster heads from the devices on the ground which may result in a cluster head whose infrastructure does not support the required level of D2D communications with all the devices in its vicinity unless additional configuration is done. Said configuration may take up valuable search and rescue time.

The above shortcomings of strategies that employ the partial or complete use of ground devices in aiding network coverage during disaster recovery operations are as a result of a phenomenon that can be summarised as ***black-box modelling*** since we simply do not have all the information about the ground devices as well the precise physical on-ground conditions. In that, we model for a strategy whose implementation still relies on a very optimistic outlook when the case at hand demands the converse. We can therefore cite the above reasons (and many more) to make a case for a strategy such as the one proposed in this study that is purely reliant on UAVs as relay nodes.

Although there has been extensive research into the use of UAV-assisted frameworks for various practical applications including disaster recovery as seen in [8], there has been overwhelming focus on framework modelling i.e., defining the optimum conditions for which UAV-assisted network enhancement can be applied as well as designing UAVs for use in disaster recovery [9, 1, 10, 2]. Along with this, we have come across research that touches on various general aspects of queuing analysis in UAV-assisted for instance, in [11] where Bisnik and Abouzeid elaborated on a queuing analysis approach for multi-hop networks. Such an approach could be instrumental in modelling queues for ad-hoc scenarios such as Flying Ad-Hoc Networks (FANETs). All these form a firm foundation for our goal to add to work that includes mobile UAV relay nodes and implements an iterative method of solving for queuing performance measures in the context of disaster recovery.

Concerning the evaluation methods utilised in this study, we can cite the inflexibility of existing proprietary software typically used for discrete event network simulations such as NS-3. As will be highlighted, the topology of the proposed model entails a communication chain comprising three different types of linked devices. An aspect in

which, unfortunately, the existing version of NS-3, for instance, is limited. Analytical models such as the one presented in this study, on the other hand, provide a more flexible playing field for queuing analysis allowing the inclusion of the required devices and heterogeneous network links in the communication chain provided the mathematical quantities are accounted for in the model. Additionally, as will be expounded on later, analytical solutions are computationally faster and cheaper on average as opposed to simulation-based evaluations [12].

1.1 Objectives of the Thesis

By the end of this study, we should have

- Discussed the *modus operandi* of the non-stationary UAV-RNs with the aim of efficiently providing wireless service for stranded mobile devices with the assistance of surviving ground base stations (BSs).
- Elaborated a two-stage queue model for D2D interaction. Consequently, the solution based on a system of simultaneous equations for solving the queuing model is looked into.
- Utilised an iterative analytical model to optimize the use of resources by expanding the model to accommodate large queue sizes and provide a computationally time-conscious solution as well as to achieve realism and to circumvent the state explosion problem that is characteristic of the solution based on a system of simultaneous equations pointed out above, . The drawback of the proposed solution, difficulty in identifying the limit of convergence, henceforth denoted as ϵ, will also be reviewed.
- Presented numerical results for the analysis of the proposed queuing model with different system characteristics and queuing capacities of systems in interaction chosen more realistically.
- Validated the proposed iterative solution for accuracy and efficacy by contrasting it with numerical results from a simulation program. To this effect, the

discrepancy between the results will be shown to adhere to the 5% confidence interval of the simulation program [12] while the system is stable to offer a post hoc justification for the application of the iterative analytical method.

- The CPU execution times of the iterative method are compared with corresponding simulation execution times to further legitimize the implementation of the former.

1.2 Thesis Contribution

Ultimately, the contributions of this study can be encapsulated as follows:

- A model is presented for the analysis of the interaction between the UEs, UAV-RNs and BSs using a two stage queuing solution with relaying and feedback for D2D communication [3] in the context of UAV-assisted wireless network enhancement in disaster recovery queuing analysis is elaborated.
- An iterative method of solving for the two-stage queue introduced in [13] by Ever at al. is implemented to optimize the use of resources by expanding the model. This solution serves to accommodate large queue sizes and provide a computationally conservative solution. Thenceforward, an augmented approach to generating the initial conditions required to kick off the iterative method is introduced.
- Adherence to the 5% discrepancy cap set in line with the simulation program's confidence interval [12] under stable conditions is depicted. The maximum (4.0212% - effect of θ_1 on BS mean queue length, MQL_{BS}) and minimum (0.000710468% - effect of primary UAV-RN service rate, μ_1 on UAV-RN throughput, γ_{UAVRN}) discrepancies recorded for the investigated performance measures are also alluded to.
- Under standard conditions, the iterative method performs better computationally in terms of execution time in seconds (with a maximum of $0.476825s$ and a minimum of $0.346084s$) against the custom simulation program (with a maximum of $317.49s$ and a minimum of $239.22s$).

- The drawback of the utilised iterative method i.e., the difficulty in identifying/approximating the limit of convergence, henceforth denoted as ϵ, is also be reviewed.

1.3 Thesis Outline

The subsequent chapters of this thesis tackle the related works and their relevance to our objectives and target contributions in Chapter 2, the system model of the proposed solution and the ensuing two-stage queuing solution in the context of disaster recovery in Chapter 3, the heavily touted iterative method implemented to solve the aforementioned two-stage queuing model in Chapter 4 and the results obtained from the iterative analytical model contrasted with a custom simulation program in Chapter 5. In Chapter 6, we tackle the limitations of this study and consequently touch on possible future works that may arise. Finally, Chapter 7 concludes the paper by reviewing the objectives and acknowledging whether or no they have been accomplished.

CHAPTER 2

RELATED WORKS

2.1 Literature Review

Having laid the groundwork by introducing the problem environment and identifying the gaps in the current research, we will explore the state of research that forms the building blocks of our proposed solution.

2.1.1 UAVs in wireless networks

In recent times, surveys [14, 8] have presented an overwhelming number of scenarios in wireless communications for which the use of UAVs could be used to improve network throughput. These surveys cite the role of UAVs as hovering BSs. In addition, emerging issues including energy trade-offs - the concept of "Green UAV communications" is tackled at length in [14], the shortcomings of using UAVs in wireless networks regarding network performance and stability of service provided, physical layer concerns for instance non-line-of-sight communications analysis [14] and the overall sustainability of UAV-based networking schemes in contrast to other more [perceivedly] fixed or permanent solutions. In all these, the inordinate sentiment is that the upsides of implementing UAV-based solutions most notably their flexibility supported by on-demand deployment, high mobility and energy efficiency [14] far outweigh the drawbacks such as limited battery power, restrictions due to no-fly zones, and safety concerns. At the very least the pros makes the work required to address the cons worthwhile.

2.1.2 UAVs in PSNs and performance evaluation

In line with the subject content of this study, a comment ought to be made regarding existing works entailing the implementation of UAV-based/UAV-assisted disaster recovery management schemes for public safety networks (PSNs). Table 2.1 below indicates the performance evaluation of proposed models in the selected literature implementing UAV-assisted schema in disaster recovery.

Table 2.1 Performance evaluation methods used in literature.

Studies	**Evaluation Method**	**Contribution**
[15]	USARSim simulation environment	A post-disaster solution for an emergency communications system established by UAVs
[16]	Custom simulation	Use of Unmanned Aerial Base Stations (UABSs) for public safety communications during natural disasters, where part of the communication infrastructure becomes damaged and dysfunctional; throughput analysis of gains that can be obtained by exploiting the mobility feature of the UAVs
[17]	Physical deployment/experimentation	A solution that entails employing unmanned aerial vehicles (serving as data mules or routers) to reduce the problems arising from faults in a sensor network when monitoring natural disasters
[18]	Better Approach To Mobile Ad-hoc Networks (BATMAN) discovery & routing protocol and augmented research testbed	Tackling key challenges to implement fault-tolerant and efficient deployments of collaborative autonomous aircraft to increase operational reliability and performance when performing aerial sensing and assessment during disaster recovery
[19]	Python software simulation and physical demo using quadrotor UAVs	A novel approach for handling a large-scale autonomous deployment of a UAV communications network for disaster recovery
[20]	3D environment rendering	Solutions to mobility management and coverage lifetime. A distributed mobility algorithm, based on the virtual spring model, through which the SUAV-based mesh node (Repairing Units) can self-organize into a mesh structure by guaranteeing Quality of Service (QoS) over the aerial link, and connecting the maximum number of ground devices
[21]	Modeling and custom simulation	A holistic and realistic framework that dynamically enables the ground users to invest their transmission power in an autonomous manner either in the UAV-based and/or MBS-based communication, while accounting for their Quality of Service (QoS) prerequisites and risk preferences. Optimizing the balance between low transmission power and high achievable data rate

As pointed out in this study, Table 2.1 supports our claim that majority of the available research is concentrated on framework modeling and presenting solutions to physical

challenges faced in the deployment of UAV-based disaster recovery networking solutions. The goal of this study is to improve on this by contributing to work pertaining explicit queuing analysis for UAV-assisted frameworks in this context.

2.1.3 UAVs as mobile pure relay nodes

In [8], the use of UAVs as mobile pure relay nodes in the context of Wireless Sensory Networks (WSNs) whereby the deployed UAVs collect information from the WSNs in the field and dump it at the central data collection point. With such a framework, the UAVs essentially replace the traditional static relay nodes that would be stationed in the fields creating a multi-hop topology that was marred with packet loss and single point-of-failure issues. Another example of the use of UAVs as mobile pure relay nodes in a highly dynamic environment is seen in [10] by Yixin et al. In this case, the deployed UAV relay node aides in communications between nodes in a Vehicular Ad-Hoc Network (VANET) by collecting packets at a source node (seemingly a vehicle initiating communication with another within the VANET) and dumping them at a sink node (the destination vehicle with whom the source was attempting to communicate). Since packet delivery is targeted, the UAV performs this operation back and forth thus allowing the VANET to circumvent issues that arise from the rapid mobility of nodes in VANETs.

Figure 2.1 below shows the mode of operation described.

Admittedly, the use of UAVs in this manner could be perceived as less intelligent and the network is likely to experience a lower throughput and higher delay [22]. However, this comes with the upside of efficient resource (energy) use in that a UAV employing a "dump-truck" approach is selectively utilising the transmission energy - only when in range of the source/destination [22] - thus consuming less energy than static relay nodes performing the job of a substitute BS which require transmission energy throughout their hovering time. Flexibility manifests itself in the form that the leeway provided for configuration of the deployed infrastructure can be modified to increase or decrease the area of coverage, velocity of the UAV or the transmission rates according to the needs of the scenario in question.

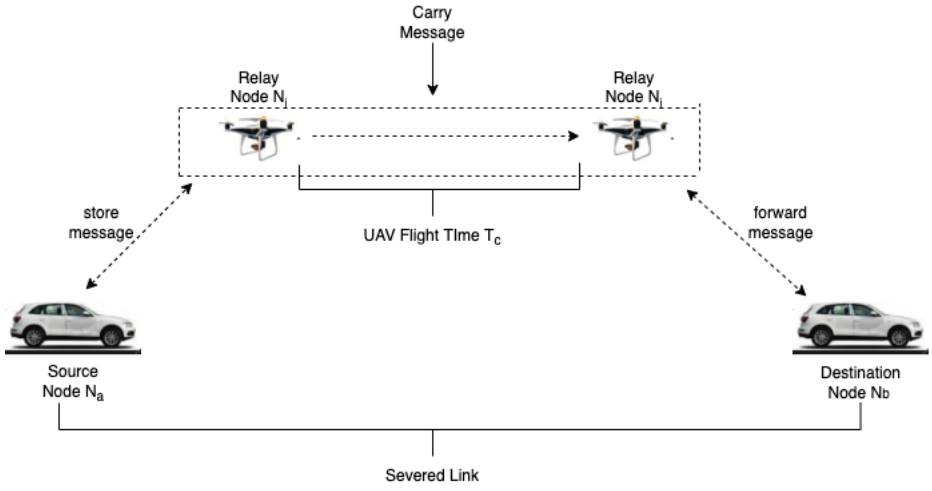

Figure 2.1 Unmanned aerial vehicle (UAV)-assisted vehicular ad-hoc networks (VANETs) architecture.

Another case of research into the use of UAV's in wireless networking applications can be cited from [9] in which Fenyu Jiang and Chris Philips successfully present a study into bettering the throughput of a UAV deployed in a disaster recovery environment much like in our case. In this paper, the authors have performed an exemplary job in relating the UAV-RN bandwidth to the throughput and UAV trajectory as a means of improving network performance. The culmination of the study is a UAV-RN trajectory planning scheme that utilises a cited Dual-Sampling method to maximise data transmission throughput. Bandwidth scheduling/contention schemes are also explored int his study. The contribution of this article to our work is in the form of the precedent of the framework parameters that we will use in our proposed model. Furthermore, it would be judicious to note that this paper is heavily invested in the mathematics of the framework (bandwidth scheduling and trajectory planning) but still falls short of mentioning any queuing analysis of the UAV-based relaying solution explored and a strong case could be made that the success of our study presents the necessary information to fill this gap.

2.1.4 Case study with on-ground RNs

The framework explored in [3] by Ever et al., is a prime example of those whose undoings we have discussed in the preceding section (1) involving the use of mobile cluster heads as relay nodes (RNs) to provide additional coverage to stranded user devices in the disaster recovery environment. As depicted in Figure 2.2 below, the ground relay nodes are devices that are within the coverage area of an operational base station while themselves providing a signal to a number of devices in their vicinity but outside of the coverage area of the operational BS. To this effect, the relay node also has its own area of coverage. The size of the area of coverage may vary depending on the strength of the signal as well as the nature of the physical location of the devices in question but it is assumed that the standard area of coverage would be significantly smaller than that of an operational base station. As discussed in the preceding section (1), these relay nodes may be selected randomly from the devices right at the border of the operational cell or [presumably] selected via an intelligent election algorithm.

Figure 2.2 below shows the system model discussed in [3].

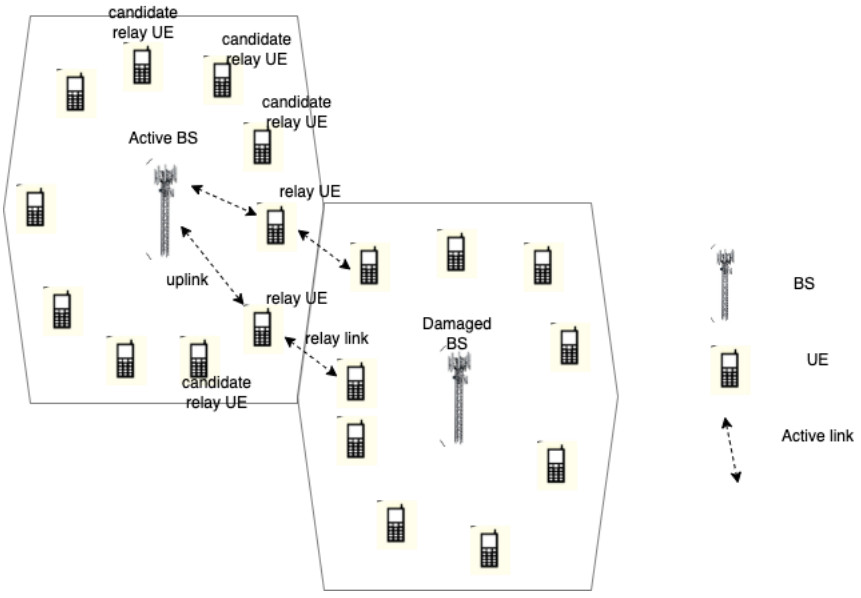

Figure 2.2 Case study with [relatively] static ground RNs.

Any device at the operational cell border could be a candidate ground relay node, de-

noted as “Relay UE” i.e., “Relay User Equipment”. In light of this assertion, another issue arises. We are not guaranteed a consistent signal strength in the event that the battery power of the current ground RN runs out. This additionally hampers search and rescue operations if the transmission strength of emergency packets within the disaster area is marred with unpredictable latencies.

As we will see in the succeeding section 3.1, this forms the basis of our proposed model and as such, will henceforth be referred to as the comparative model.

2.1.5 Two-stage queuing

We present this in two parts:

1. **Flat/Generic two-stage queuing**; In [3], the queuing model presented is a two-stage tandem queuing system shown in Figure 2.3 below.

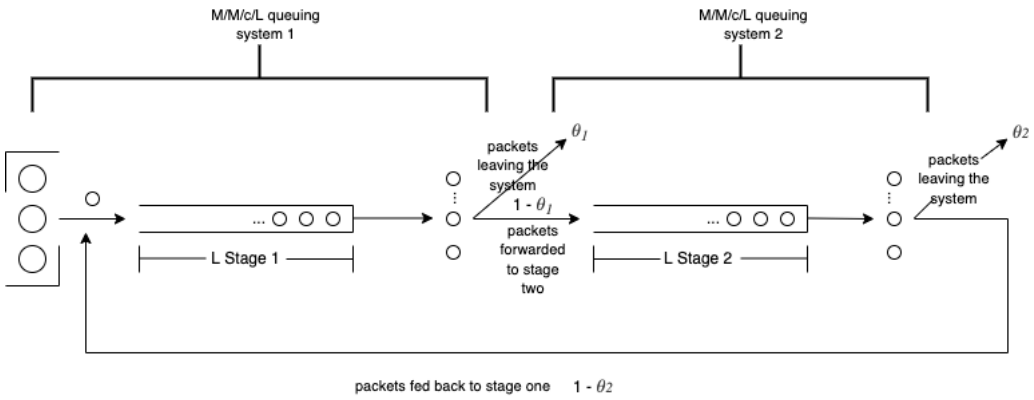

Figure 2.3 Two-stage M/M/c/L tandem queuing with feedback.

The queuing system used is a Markov model denoted with Kendall’s notation [23] to indicate exponentially distributed inter-arrival and service times, multiple servers i.e., channels, and limited queue sizes. The other parameters of the notation such as the infinite pool of packets and the queuing discipline (First-In-First-Out) are implicit.

In this model, the first queuing stage is for packets received from the stranded mobile devices by the relay node, hence the stage is referred to as “uplink

stage". In the second stage, the received packets are subsequently forwarded to the operational BS in whose area of the coverage the RN is. This stage is hence referred to as the "relay stage".

It is also important to note that the queuing model takes into account packet loss probability i.e., probability that the packet is not forwarded to the relay stage (denoted by $1 - \theta_1$) between the uplink and relay stages as well as the feedback probability (denoted by θ_2) when the packets are fed back from the relay stage to the uplink stage.

The framework proposed in [3] by Ever et al. aims to provide continuous cell signal for voice and data communications to stranded devices in the disaster area. While ideally this would be a very helpful, the practicality of it could be perceived as too optimistic and inefficient in the use of resources in terms of energy concerns with regard to the relay nodes as well as the devices receiving the signals themselves. This study presents an analytical model and an accompanying simulation to evaluate the proposed framework.

2. **Two-stage queuing in the context of heterogeneous networks**; In [12], Yaqoob et al. investigates a scheme that is aimed at improving network speed by introducing a 5G femtocell in a 4G macrocell.

   The resulting framework also calls for the use of a two-stage tandem queuing model. Unlike in [3] by Ever et al., the proposed tandem queuing model employed in this paper constitutes tandem Markov queues i.e., an M/M/c/L queue followed by an M/M/1/L queue, as shown in Figure 2.4 below.

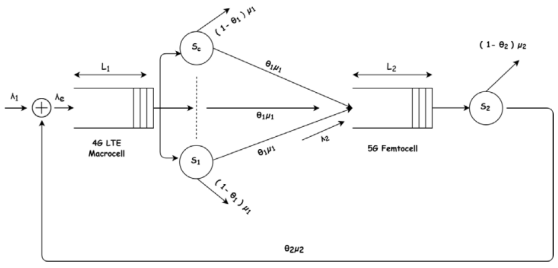

Figure 2.4 Two-stage M/M/c/L->M/M/1/L tandem queuing with feedback.

Following Kendall's notation for queue description [23], the proposed queuing

model by Yaqoob et al. has exponentially distributed inter-arrival and service times, multiple servers (channels denoted S_1 to S_c, where $\boldsymbol{c}$ is the number of channels in the 4G LTE macro-cell) in the first stage, one server (channel) at the femto-cell stage; and limited queue sizes (denoted by L_1 and L_2 respectively). The size of the packet pool and queuing discipline are not indicated but are implicit as is the case in [3].

It is vital to note that in this model, an effective lambda value (denoted by λ_e) is utilised for the packet arrival rate of the first stage in line with the proposed product form solution investigated in the paper. This is one of the mathematical contributions of this paper to our own proposed solution. Similar to the model explored in [3] in Figure 2.3 above, this model accounts for packet loss probability i.e., the probability that the packet is not forwarded to the femto-cell queue (also denoted by $1 - \theta_1$) and feedback probability (also denoted by θ_2).

This paper provides important precedent on three fronts;

- It provides a suitable example of implementation of two-stage queue modelling for wireless networking with packet forwarding and feedback.
- This study presents an analytical solution based on a system of simultaneous equations which is improved upon by introducing a product form solution as well as an accompanying custom simulation to evaluate the proposed framework.
- It presents the necessary groundwork for queue modelling in heterogeneous wireless networks which is very handy with the rapid rise in future generation networks. This enables research and application of solutions to be done in parallel with production of new technologies.

  The contribution of this to our model is that it enables us to circumvent the problem of interoperability. In the event that the disaster area is operating on or only has surviving infrastructure that is of a previous generation, we can still provide a relay link by retrofitting the UAV relay node necessarily and deploying it to the stranded zone, further strengthening the argument for our proposed framework.

2.1.6 Rudimentary solutions for multi-stage queuing

In this subsection, we present precedents for the preliminary analytical solutions put forward for two-stage queuing systems. These solutions, albeit accurate, are severely computationally limited both temporally and spatially especially under realistic conditions. The limitations arise from the use of system of simultaneous equations to solve for state probabilities. Support for this is availed by two instances:

1. In the context of heterogeneous networks; In [12], the two-stage tandem queuing model obtained from the proposed framework results in a 2D state transition diagram to track the behavior of the model given various stimuli. As we will later see in our own study, the state transition diagram is vital in the derivation of the balance equations needed to calculate the state probabilities for each region in the state transition diagram. Akin to the framework modelling precedent alluded to in the previous point, the paper by Yaqoob et al. allows us to proceed with this approach in solving for state probabilities for our model even if we would like to adapt our model for heterogeneous cases.

2. Comparative case study; The approach used to solve for state probabilities in [3] by Ever et al. is also a solution based on a system of simultaneous equations. We have not elaborated this solution here because it is part of our model and as such, will be explained in the preceding section (1).

2.1.7 Iterative solutions for multi-stage queuing

In [13] by Ever et al., we are presented with an approach that allows us to circumvent the touted solution based on a system of simultaneous equations which may deem to be computationally heavy when realistic parameters are applied. The solution explored in this paper provides a relief from the state explosion problem that is characteristic of two-dimensional Markov processes.

The general idea involves expressing the state probabilities in terms of surrounding state probabilities. The state probabilities are then initialized, taking into account the

parameters of the model in question (hence why we have highlighted the forwarding/packet loss and feedback probabilities while discussing [3] and [12] and their contributions to our study). This is the most important part of the solution as the initial conditions must be such that the rules of Markov processes/models and probabilities as a whole are not violated at the end of the procedure. After initializing the state probabilities, the calculations used to obtain them for every region of the 2D state transition diagram are performed in a loop until a convergence on the MQL values is achieved based on the chosen limit of convergence, ϵ.

The resulting state probabilities are then used to calculate the queuing performance measures of the proposed network. In [13], the iterative solution presented is successfully applied to a 3D Markov process with tremendous accuracy and proved to be computationally light in comparison to the solution based on a system of simultaneous equations explored for the same scenario.

2.1.8 Energy modeling and evaluation in wireless networks

In [24] by Ever et al., an energy consumption model is presented for WSN cluster heads. The energy model is broken down into, transmission, receipt, idle and sleep states in each of which the cluster head is expected to expend energy. The proposed energy model in the study elaborates a model that is subject to the state, rate of transmission or reception and the mean amount of energy required to receive a packet at or transmit a packet from the cluster head. In our case with UAV-RNs, we can adapt this energy model to suit our scenario to calculate the approximate amount of energy we expect a deployed UAV-RN to consume seeing as we envision the UAV-RNs to have transmission, reception and idle states.

Additionally, in [25] by Abeywickrama et al., we are presented with an already validated energy consumption model for UAVs in the context of communication. While the UAVs in this study are not being used as relay nodes, we can still adapt the energy models put forward for the various modes of the UAV and bootstrap our model by augmenting the transmission and reception energy consumption quantities to cater for our case and account for relaying and feedback as well.

2.1.9 Research gaps

To this point, we have presented the building blocks of the work tendered by our own study. It can therefore be gleaned from this that there is room for improvement in the research available regarding explicit analysis of workable solutions presented for the use of UAVs as RNs in disaster recovery, both in terms of the queuing and consequent efficient analytical solution as well as energy consumption modelling in this context.

CHAPTER 3

SYSTEM MODEL

Having presented the problem definition and highlighted the shortcomings of the available solutions, we will now provide what we deem to be an alternative solution that aims to address the hitherto mentioned problems and overlooked crevices in the current research.

This chapter is organised such that, we will first describe the role of the UAVs relay nodes deployed in the disaster area. We will attempt to provide existing infrastructure/research to further support the feasibility of the proposed framework after which we will present the queuing model, the subsequent derivations and accompanying popular solution based on a system of simultaneous equations.

3.1 The Proposed Framework

In line with the comparative case study proposed in [3] and shown in Figure 2.2, the physical positioning of the relay node in the disaster area is of utmost importance. The optimum location would be one that achieves equal signal strength for both uplink and relay stages of the packet lifetime. Additionally, the heretofore much touted rapid mobility of the UAV relay node is achieved by the UAV circulating the stranded cell at an optimum speed that balances area coverage while not compromising packet delivery. The area of coverage of the UAV relay nodes deployed in the proposed framework are in the quintessential conical shaped as seen in the Figure 3.1 below from [2].

Although we borrow the shape of area of coverage from [2] by Mozaffari et al., we maintain the hexagonal shape of the cell that is commonly assumed for wireless networks. This way we are able to plan for a definite number of neighbouring cells in our

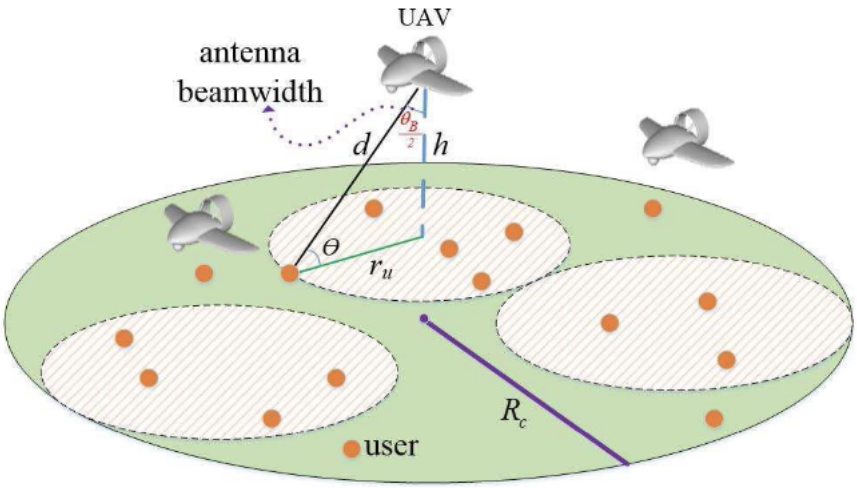

Figure 3.1 Conical shaped area of coverage of deployed UAV relay nodes [2].

proposed framework. In line with [26], we can also make the educated recommendation that the proposed framework should be implemented using fixed-wing UAVs in lieu of the traditional rotary UAVs used in schemes that are dependent on the UAVs hovering. Fixed wing UAV relay nodes would be better suited for this scenario due to their small size; their relatively smaller size translates to less energy required to fly them at varied altitudes if the need arises, high speed, ability to carry high payload and can fly for several hours.

The dimensions to scale of the radius of the area of coverage, denoted as r_u in Figure 3.1 (coincides with the dimension ***r*** in Figure 3.2) indicates that this value is expected to be less than or equal to the length of the side of the hexagonal-shaped cell such that the UAV provides optimum coverage to the stranded devices at this region of the cell while avoiding provision of redundant coverage to the devices in the next region (of the same cell) that it is going to traverse.

Figure 3.2 shows an ideal placement of the UAV relay node at the border between two cells. We deem this to be the ideal positioning because at this position, the UAV-RN is still within the area of coverage of the operational base station while providing continuous coverage to as many ground UEs as possible in the stranded

cell. Consequently, Figure 3.3 below shows the *modus operandi* of the proposed framework when all the above details are taken into account.

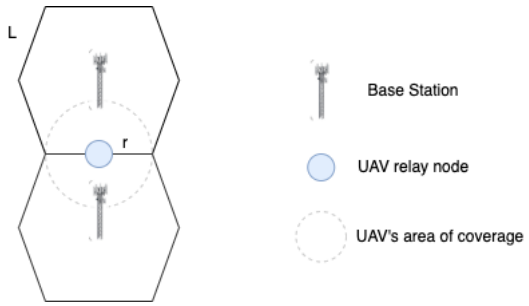

Figure 3.2 Ideal UAVRN placement in the proposed framework.

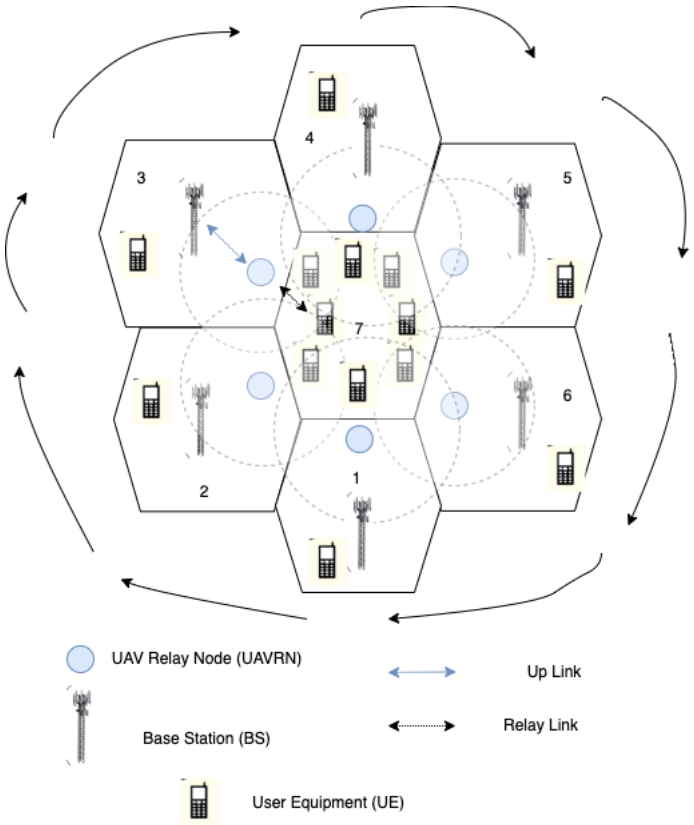

Figure 3.3 Proposed framework with highly mobile UAV-RN.

As indicated in Figure 3.3 below, the deployed UAV relay node traverses the disaster area in a clockwise direction i.e., while servicing stranded cell 7, starting at the border of cell 1 (and 7), moving to the border of cell 2 (and 7) and so on providing **continuous** coverage to the devices in the stranded cell until the revolution is com-

plete and the UAV-RN is back at the starting point. The idea is that the emergency SOS packets (discussed ahead) broadcast by the stranded devices and relayed to the emergency channel of the operational base station are then accessed by the search and rescue authorities to aid in locating device holders in the localised disaster area. This process is repeated until the search and rescue operation is completed.

For this framework to achieve realism as well as to simplify the mathematics we need to perform the analysis, we shall make the following assumptions:

1. Packets: Since we have lauded the energy-friendly nature of this framework, it does not aim to provide voice and data needs to the devices in the stranded cell. Instead, compact emergency SOS packets that require significantly less energy to transmit (by both the devices and the UAV-RN). The SOS packets consists of the device's serial number - 16 bytes, the GPS location/coordinates - 6 bytes - and the timestamp (date and time in hours, minutes & seconds) - 13 bytes. This gives us an estimate of about 35 bytes per packet in comparison to the average data packet that is 1000 to 1500 bytes long [27]. Computationally, this translates to one data string per device hence allowing the channel to hold a considerably large number of packets within a very short period of time without causing a bottleneck. Additionally, the compactness allows some leeway in packet handling in case there are some duplicate packets received due to redundant coverage i.e., when the UAV-RN receives an SOS packet from the same device in the same sub-cell during one revolution.

2. The stranded devices have SOS capabilities: This feature already exists for most if not all current smart devices. At the very least as per 5G (seeing as this is one of the target network infrastructures for this framework, we are able to use its device density estimates) research [28], it is expected that there will be at least one smart device with SOS capabilities in every square metres (10^6 devices per square kilometer). This maintains the high probability that a stranded individual is within a reasonable distance from a device that is broadcasting SOS packets in the event that some devices are rendered physically unable to broadcast the SOS packet.

3. There is at least one neighboring cell with an operational base station: As seen in Figure 3.3 above, the framework is dependent on continuous provision of coverage. Consider a situation in which the BSs in cells 2, 4 and 6 are also down. The compact nature of the SOS packets described in (a) above allow the UAV-RN to hold the packets collected from the sections of the cell adjacent to cells 2, 4 and 5, and relay them to the operational BSs in cells 1, 3 and 5.

4. Variable velocity path training: Though highly optimistic (or pessimistic depending on your point of view), in line with the above point (c), this scheme would be even more effective with variable velocity path training as proposed in [29] by Rui Han et al. for UAV application in IoT environments. With this enhancement, the UAV-RN velocity can be altered depending on the load size that needs to be relayed to the operational BS. This could come in handy when a significant number of the neighbouring BSs are down and the fail-safe implemented by the compactness of the SOS packets discussed in (a) is not enough to relieve the UAV-RN. The velocity can be lowered from the optimum to allow the RN to dump the packets in its queue and restored to the optimum once all the packets have been relayed. We however envision this to be the absolute worst case owing to the computationally light SOS packets in the proposed framework.

5. Variable altitude path training: This would be a more advanced strategy to guard against queuing bottleneck. The proposed implementation in [2] allows us to control the number of devices within the area of coverage by varying the altitude of the UAV relay node during its flight. When the queue length is approaching a critical point, it is possible to lower the altitude of the UAV (provided the altitude is still safe enough for the flight path of the UAV to be unobstructed). This means that less packets would be arriving at the UAV per unit time while maintaining the transmission rate at a constant. Indeed there is the trade off that the UAV would expend less energy flying at this low altitude but the time it would take to traverse the length of the cell would cancel out this effect.

6. The stranded mobile devices are always broadcasting the SOS packets in a

heartbeat rhythm (the broadcast rate of the ground devices i.e., arrival rate of packets to the UAV-RN will be discussed in the next subsection - 3.2) as long as they are on.

7. The ground device broadcasting scheme is not such that the devices are synchronised to broadcast the SOS packets simultaneously, rather it is arbitrary. To this effect, the primary arrival rate at the UAV-RN stage, λ_1 (whose mathematics is extensively discussed in the next subsection - 3.2), say $\boldsymbol{x}$, is essentially predicated on the assumption that per unit of time, $\boldsymbol{x}$ devices within the range of the UAV-RN's area of coverage are broadcasting their respective SOS packets; and not that there are $\boldsymbol{x}$ number of devices in the UAV-RN's area of coverage.

8. The UAV-RN receiving channel is always listening for a connection with the stranded devices on the ground. Upon establishment of connection, the packets are received as long as they are being broadcast (as per point number 6).

9. The stranded devices are uniformly distributed throughout the cell. This assumption is of mathematical importance to the queuing model that accompanies this proposed framework; as will be made abundantly clear in the next subsection (3.2).

10. The packet handling scheme at the Base Station end-point is intelligent enough to eliminate duplicate SOS packets received due to originating packets (those within the coverage area of the operational base station) being in the area of coverage of the UAV-RN. At the very least, the packet handling at the UAV-RN uplink stage ought to be such that only the devices in the stranded region that were assigned to the destroyed BS (this is possible since in Mobile IP, devices are assigned to a BS as a home agent [30] in a cell) are able to join the queue, with packets from any other devices being discarded. Such an implementation would significantly reduce energy consumption and time that would have otherwise been wasted in sorting redundant packets.

11. The operational base stations in the disaster area transmit a feedback packet acknowledging receipt of the UAV-RN's payload. This is a vital part of the queuing model discussed in the succeeding section (3.2) and as such, is worth

paying close attention to.

The advantage of the proposed framework is vivid in the following respects:

1. **Energy**; Albeit outside of the scope of the specified contributions of this study, we can make an inference on the projected benefit of the proposed model as pertaining energy consumption. The SOS packets used in the proposed framework would require a lot less transmission power; a variable velocity scheme such as the one alluded to in the assumptions above could be implemented for regions of the cell containing fewer stranded devices; in the event that several cells (especially if they are scattered with operational cells in their midst) fewer number of UAVs could be used for the same number of cells in comparison to traditional schemes that utilise dedicated hovering UAVs for each stranded cell [1].

2. **Continuous coverage**; Considering the mobile relaying scheme implemented in Figure 2.1, packets are collected at the source and dumped at the destination by the UAV-RN. In between i.e., the time during which the UAV-RN is dumping the packets at the destination and collecting the feedback packets to deliver back to the source node, there is some communication latency that is experienced. As will be cited in the rationale for the proposed queuing model to be discussed in the next subsection (3.2), the immensely lightweight nature of the SOS packets allows for the use of a dedicated emergency channel on the operational base station/s without interfering (or at least to a noticeable extent) with the performance of the other channels being used for normal (data and voice) communications by devices in the coverage area of the operational BS but outside the localised disaster area. In light of this, continuous coverage is being offered to originating devices as well as the stranded devices.

3. **Preemptive load balancing**; This applies in both what we shall now refer to as the optimistic condition (that in which all neighboring cells have operational base stations) and when some of the surrounding (with respect to the cell of interest) base stations are down as well. In traditional schemes such as the

one depicted in Figure 1.1, the destination of the packets is a dedicated emergency communication vehicle (ECV) or a neighbouring operational base station. Granted that these frameworks may not be implementing the same SOS packet scheme as our proposed strategy hence the need for a dedicated destination, this creates a single point of failure; and search and rescue operations would be jeopardised should any harm come to the BS or the ECV.

4. **Scalability**; This scheme enables the deployment of targeted infrastructure to the stranded cell in comparison to traditional implementations of relay nodes [3] that are limited to available ground devices. For the latter strategy, it is highly probable that the assigned resources may be under-utilised or over-utilised. In the proposed framework, search and rescue authorities have the luxury of deploying smaller/less energy-intensive relay nodes as more and more people are rescued.

3.2 Queuing Model

In this study, an analytical model is also presented to investigate the queuing performance of the proposed framework discussed at length in the preceding subsection.

In this subsection, we will discuss the queuing model, existing applications of the model's building blocks as seen in the chapter on "Related Work" as well as the common solutions for the model. We will then solve the model using the matrix method in this section and attempt to shed light on its advantages and drawbacks.

In Figure 3.1, in which we are presented with the MO of the proposed model, when the UAV relay node is positioned at the border between cell 3 and cell 7 (the stranded cell).

When the UAV is within range of both the stranded devices on the ground and an operational base station, we envision a queuing model that involves SOS packets being received from the stranded devices and relayed to the operational BS. Simultaneously, the operational base station will be servicing the devices in its own area of coverage. Additionally, we visualize the base station responding to the UAV relay node with

a feedback packet acknowledging reception of the payload. This introduces the proposed two-stage tandem M/M/1/L Markov queuing model shown in Figure 3.4 below.

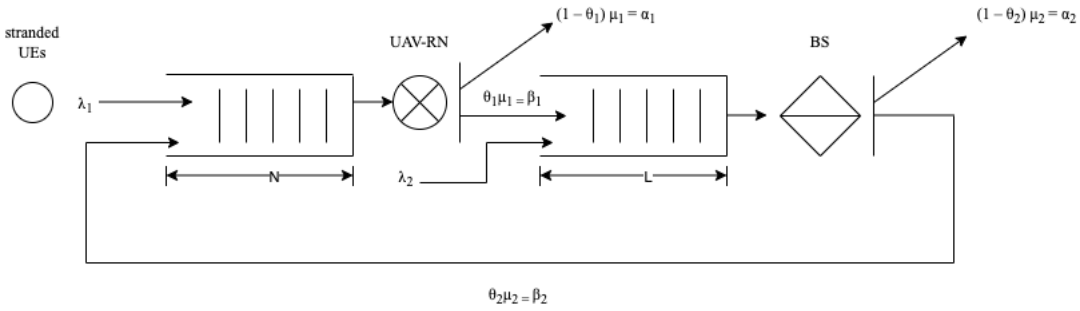

Figure 3.4 Two-stage queuing model with feedback for the proposed framework.

NB: the term "User Equipment(s)", denoted "UEs" throughout this study, refers to any connected mobile devices on the ground.

The rationale behind implementing the model with M/M/1/L queues can be traced back to the pros of the proposed framework cited in the previous subsection (3.1):

- Energy concerns; The compact SOS packets already allow us the leeway to service a large number of devices per unit time (as we will see in the analysis of the performance measures), thus rendering multiple servers (which would translate to multiple channels in the UAV relay node/BS) redundant. More channels require more energy consumption; this would be antithetic to the objective of the proposed framework.

These parameters, whose notations are matched with their respective definitions in Table 3.1, are explained as follows:

1. Arrival rates; The two-stage queuing model comprises two types of arrivals, primary arrival (of packets **originating** from the cell) and secondary arrival (of packets forwarded from either stage). As is the case in [12, 31], inter-arrival times for primary arrivals, denoted as λ_1 and λ_2 for stages one and two respectively, are exponentially distributed. Secondary arrivals are denoted as $\theta_1\mu_1$ (contracted to β_1 for simplicity) for stage one and $\theta_2\mu_2$ (contracted to β_2 for

Table 3.1 Notations and their definitions

Notations	Definitions (trace-based)
λ_1	Mean arrival rate at the UAV relay node (from stranded UEs)
λ_2	Mean arrival rate at the (operational) Base Station (from its assigned ground devices)
μ_1	Mean service rate at the UAV relay node
μ_2	Mean service rate at the (operational) BS
θ_1	Probability of packet forwarding at the UAV-RN stage
θ_2	Probability of packet feedback at the operational BS stage
$\theta_1\mu_1$	Forwarding **rate** of packets from stage one (UAV-RN) to stage two (BS)
$\theta_2\mu_2$	Feedback **rate** of packets from stage two (BS) to stage one (UAV-RN)
$(1-\theta_1)\mu_1$	Departure **rate** of packets from stage one (due to packet loss)
$(1-\theta_2)\mu_2$	Departure **rate** of packets from stage two (due to service completion)
u_1	System utilisation/non-idle time portion at stage one
u_2	System utilisation/non-idle time portion at stage two
γ_1	System throughput at stage one
γ_2	System throughput at stage two
N	Queue capacity at the UAV-RN stage
L	Queue capacity at the operational BS stage
ϵ	Limit governing convergence (in the iterative solution, Chapter 4.3)

simplicity) for stage two. The numerical quantities of these values is assumed to be constant in line with the assumption asserting the uniform distribution of UEs on the ground. Arriving packets are serviced as long as the channel is free, else the packets join the respective queue and wait their turn.

2. Service rates; Similar to [12, 32], service times are exponentially distributed and the service rates for stage one and two are denoted by μ_1 and μ_2 respectively. Packets from stage one may be forwarded to stage two with the probability θ_1 as indicated in Table 3.1 with the forwarding rate hence being the product of the forwarding probability and the service rate at this stage i.e., $\theta_1\mu_1$; or the packets may depart due to loss (though due to the compactness of the packets, we envision that this will seldom happen) with the probability $(1-\theta_1)$ and the departure rate due to loss being $(1-\theta_1)\mu_1$ as indicated in Table 3.1.

3. Forwarding probabilities; θ_1 and θ_2 for stages one and two respectively as explained under service rates in Table 3.1 above.

4. Packet departure; $(1-\theta_1)$ and $(1-\theta_2)$ for stages one and two respectively as

explained under service rates in Table 3.1 above.

5. Queue lengths; N denotes the queue capacity of the first stage while L denotes the queue capacity of the second as indicated in Table 3.1 above.

Since we envision the proposed framework itself to be feasible for use in a heterogeneous network environment, we can go ahead and follow the same modelling blueprint as in [12] for the resulting two-dimensional Markov processes used to represent the tandem system shown in Figure 3.4. These processes can be expressed on a finite or semi-finite lattice strip. We can define the Markov process by $Z = [I(t), J(t)]$ for $t \geq 0$ having a state space of size $[0, 1, 2, ..., N] \times [0, 1, 2, ..., L]$ [12, 31, 33].

After defining the two-dimensional Markov process, it is possible to use Z (defined above) which gives us an irreducible Markov processes to represent the number of packets in the UAV-RN and BS queuing stages respectively. The state diagram shown in Figure 3.5 represents the transitions clearly.

In the state transition diagram, the system state is denoted/described by the variables i (the instantaneous number of packets in the UAV-RN stage of the tandem queues) and j (the instantaneous number of packets in the BS stage of the tandem queue). The horizontal transitions represent a change in the first stage while vertical transitions represent a change in the second stage.

For a rough idea of the logic of the transition diagram consider the state labelled (i, j) in Figure 3.5, the upward transition would increment j, i.e., the number of packets/jobs in the second stage of the queue, while maintaining i, i.e., the number of packets/jobs in the first stage of the queue. This translates to an originating packet within the cell of the operational base station, i.e., a primary arrival in the second stage denoted by λ_2 as explained in Table 3.1. This transition logic is spawns the two-dimensional lattice that allows us to trace the behaviour of our queuing model given different stimuli denoted in Table 3.1.

We can now go ahead and derive the balance equations used to mathematically express the state probabilities, $P(i, j)$, for each region of the state transition diagram.

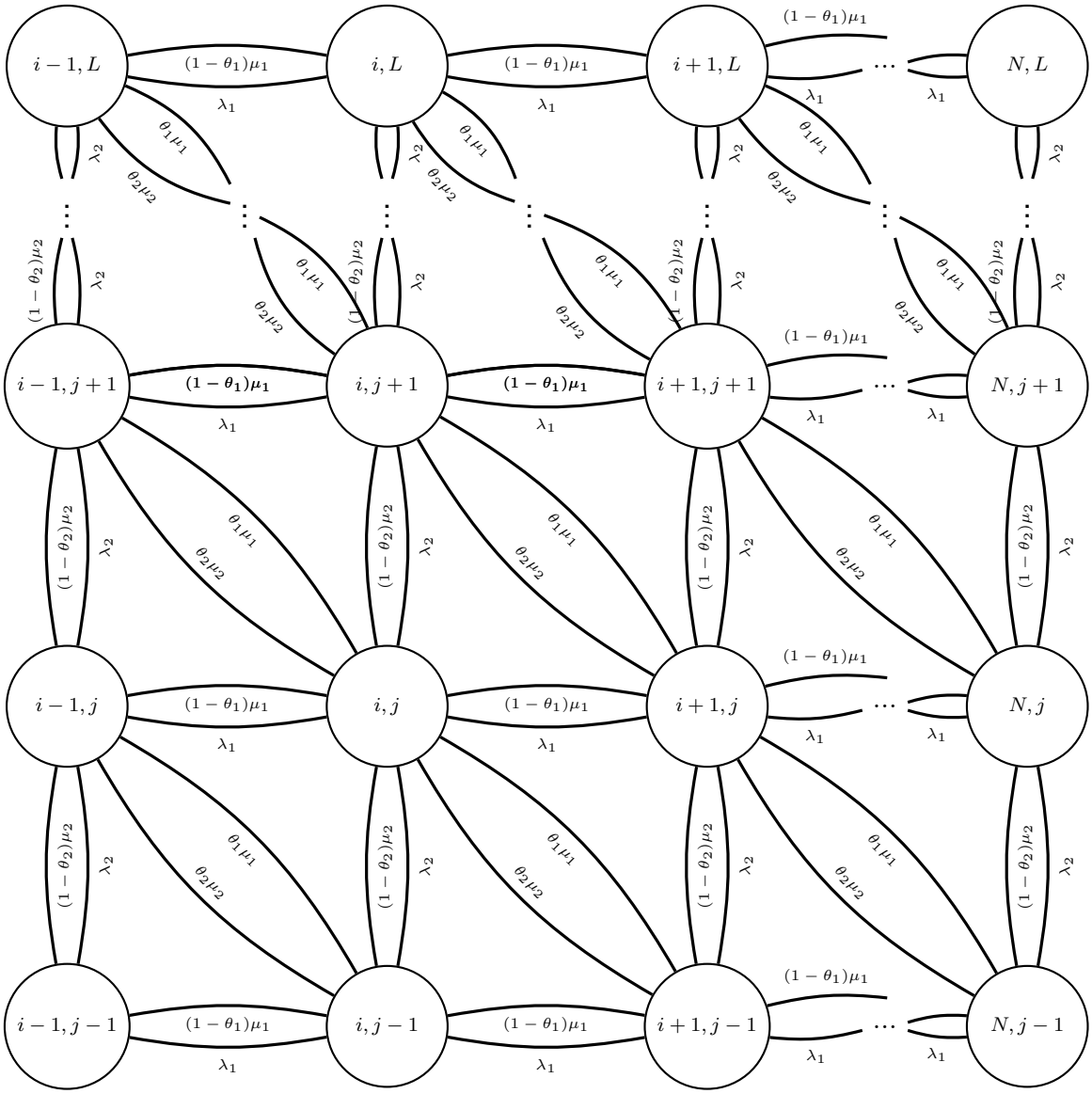

Figure 3.5 State transition diagram for two-dimensional Markov processes.

Equating the outgoing transitions with the incoming transitions in each state, the state probabilities can be expressed as follows; Region 1: where $\boldsymbol{i} = 0, \boldsymbol{j} = 0$

$$P_{i,j} = \frac{P_{i,j-1} * \alpha_1 + P_{i-1,j} * \alpha_2}{\lambda_2 + \lambda_1}$$

but i and j are both **0** in this region hence this can be expressed as;

$$P_{i,j} = \frac{P_{i+1,j} * \alpha_1 + P_{i,j+1} * \alpha_2}{\lambda_2 + \lambda_1} \tag{31}$$

Region 2: where $\boldsymbol{i}$ = 0, $\boldsymbol{j}$ = L (maximum capacity for the relay stage);

$$P_{i,j} = \frac{P_{i,j-1} * \lambda_2 + P_{i+1,j} * \alpha_1 + P_{i+1,j-1} * \beta_1}{\lambda_1 + \beta_2 + \alpha_2} \tag{32}$$

Region 3: where $\boldsymbol{i}$ = N (maximum capacity for the up-link stage), $\boldsymbol{j}$ = L (maximum capacity for the relay stage);

$$P_{i,j} = \frac{P_{i-1,j} * \lambda_1 + P_{i,j-1} * \lambda_2}{\alpha_2 + \alpha_1} \tag{33}$$

Region 4: where $\boldsymbol{i}$ = N (maximum capacity for the up-link stage), $\boldsymbol{j}$ = 0;

$$P_{i,j} = \frac{P_{i-1,j} * \lambda_1 + P_{i-1,j+1} * \beta_2 + P_{i,j+1} * \alpha_2}{\alpha_1 + \beta_1 + \lambda_2} \tag{34}$$

Region 5: where $\boldsymbol{i}$ = 0, 0 < $\boldsymbol{j}$ < L (maximum capacity for the relay stage);

$$P_{i,j} = \frac{P_{i,j+1} * \alpha_2 + P_{i+1,j} * \alpha_1 + P_{i,j-1} * \lambda_2 + P_{i+1,j-1} * \beta_1}{\beta_2 + \lambda_2 + \lambda_1 + \alpha_2} \tag{35}$$

Region 6: where 0 < $\boldsymbol{i}$ < N (maximum capacity for the up-link stage), $\boldsymbol{j}$ = L (maximum capacity for the relay stage);

$$P_{i,j} = \frac{P_{i,j-1} * \lambda_2 + P_{i-1,j} * \lambda_1 + P_{i+1,j} * \alpha_1 + P_{i+1,j-1} * \beta_1}{\alpha_1 + \lambda_1 + \beta_2 + \alpha_2} \tag{36}$$

Region 7: where $\boldsymbol{i}$ = N (maximum capacity for the up-link stage), 0 < $\boldsymbol{j}$ < L (maximum capacity for the relay stage);

$$P_{i,j} = \frac{P_{i-1,j} * \lambda_1 + P_{i,j-1} * \lambda_2 + P_{i,j+1} * \alpha_2 + P_{i-1,j+1} * \beta_2}{\lambda_2 + \alpha_1 + \alpha_2 + \beta_1} \tag{37}$$

Region 8: where 0 < $\boldsymbol{i}$ < N (maximum capacity for the up-link stage), $\boldsymbol{j}$ = 0;

$$P_{i,j} = \frac{P_{i-1,j} * \lambda_1 + P_{i,j+1} * \alpha_2 + P_{i+1,j} * \alpha_1 + P_{i-1,j+1} * \beta_2}{\alpha_1 + \lambda_2 + \lambda_1 + \beta_1} \tag{38}$$

Region 9: where $0 < \boldsymbol{i} <$ N (maximum capacity for the up-link stage), $0 < \boldsymbol{j} <$ L (maximum capacity for the relay stage);

$$P_{i,j} = \frac{P_{i,j-1} * \lambda_2 + P_{i-1,j} * \lambda_1 + P_{i-1,j+1} * \beta_2 + P_{i,j+1} * \alpha_2 + P_{i+1,j} * \alpha_1 + P_{i+1,j-1} * \beta_1}{\alpha_1 + \beta_1 + \lambda_2 + \lambda_1 + \alpha_2 + \beta_2} \tag{39}$$

All possible states in the lattice fall under one of the above nine regions whose state probabilities are expressed in Equation (31) to Equation (39).

3.2.1 System of Simultaneous Equations Solution

We can now go ahead and solve for the $(N + 1) \times (L + 1)$ state probabilities using the system of simultaneous equations. **A** is defined as matrix of instantaneous transition rates from state (i, j) to state (N, L) and holds the coefficients of the system of simultaneous equations of all state probabilities.

Once the matrix **A** containing the coefficients of the equations from each $P(i, j)$ is obtained, we can solve for the state probabilities matrix by solving the equation **AX = B**, where the matrix **X** holds the state probability variables ($P_{i,j}$'s) and matrix **B** holds the result of the equations (in our case, this matrix will hold zeros for all the equations except the last one for which the sum of all $P_{i,j}$'s is 1). The culmination of this operation is the matrix of $(N + 1) \times (L + 1)$ state probabilities from which we can then calculate the mean queue lengths.

In this study we have used the effective *numpy* libraries in Python to implement this particular method and solve for state probabilities from the system of simultaneous equations..

As alluded before, the implementation of the solution based on a system of simultaneous equations requires solving the system of $(N+1)\times(L+1)$ simultaneous equations to obtain the $(N+1)\times(L+1)$ state probabilities. Although the performance measures computed by using this solution are within the desired error margin of 5% consistent with the confidence interval of the simulation program [12], the method proves to be severely computationally heavy for queue sizes above $(150 + 1) \times (150 + 1)$. To this

effect, we shall introduce a more computationally sound iterative solution in the next Chapter (4).

Indeed, an argument could be made for the feasibility of this solution based on a system of simultaneous equations in our proposed framework. Consider the cell structure depicted in Figure 3.3. The proposed framework effectively divides the stranded (middle cell depicted having a downed base station) cell into sub-cells as shown in Figure 3.6 below.

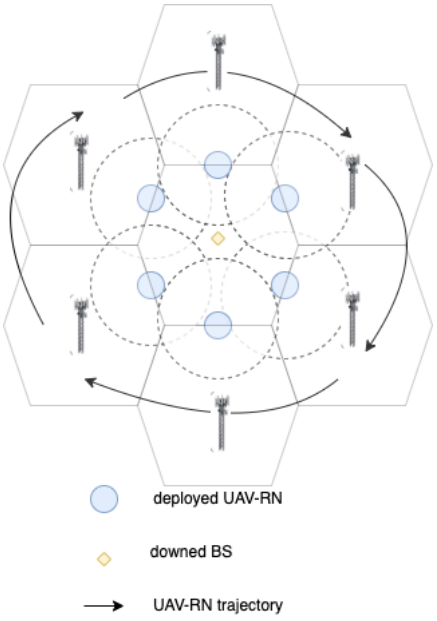

Figure 3.6 Division of stranded cell into sub-cells.

NB: The dotted lines in Figure 3.6 are the UAVs area of coverage/range. It is also imperative to remember that the UAV-RN does not hover as in traditional schemes [8], it is continuous motion.

Taking the radius of the UAV relay node's area of coverage as 1km [34] (for high end UAVs, this can value be altered for efficiency depending on the needs at hand) and the radius of the cell presumably in an urban area as 1km [35], we can work under the assumption that the queue capacities defined as N and L for the up-link and relay stages respectively coincide with a sub-cell as seen in Figure 3.6. To this effect, the proposed queuing model that is solved using the hitherto described system of simultaneous equations method is feasible for up to 150×6 (number of sub-cells)

devices in the localised disaster area.

CHAPTER 4

THE ITERATIVE SOLUTION

Having presented the queuing model and an accompanying solution, it would be prudent to expand the queuing solution to fit a more realistic implementation.

The general procedure for the iterative solution [13] can be given as follows:

1. Initial conditions for $P(i, j)$ for $i = 0, 1, 2, 3, ..., N$ and $j = 0, 1, 2, 3, ..., L$ are calculated using Markov process logic for M/M/1/L queues.
2. The balance equations given in Equation (31) to Equation (39) are used to calculate the correct steady state probabilities.
3. Mean queue length is calculated for the queuing system considered.
4. Second and third steps are repeated until the mean queue length converges sufficiently as per the chosen limit of convergence, ϵ.

4.1 Initial Conditions

Consider the example with state transition diagram shown in Figure 4.1 below for a simple Markov M/M/c/L queue with Markov exponentially distributed inter-arrival times and service times, three servers ($c = 3$) and limited queue capacity (denoted as L). The unspecified parameters (following Kendall's notation [23]) are implicit.

Taking constant arrival (λ) and service (μ_i's, for $1 \leq i \leq c$) rates, we can derive the state probabilities as follows;

$$\lambda P_0 = \mu_1 P_1; P_1 = \frac{\lambda}{\mu} P_0; P_1 = \rho P_0 \tag{41}$$

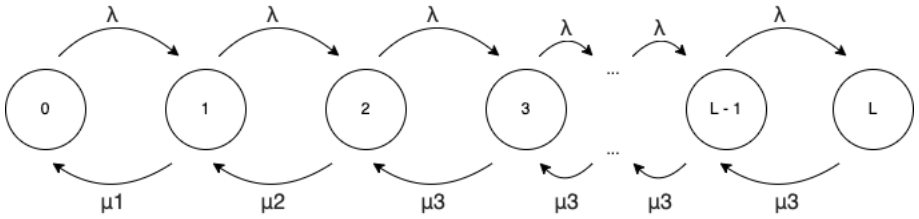

Figure 4.1 State transition diagram for M/M/c/L queue.

because

$$\frac{\lambda}{\mu} = \rho$$

$$\lambda P_1 = 2\mu P_2; P_2 = \frac{\lambda}{2\mu} P_1; P_2 = \frac{\lambda}{2\mu} \rho P_0; P_2 = \frac{1}{2}\rho^2 P_0 \tag{42}$$

$$\lambda P_2 = 3\mu P_3; P_3 = \frac{\lambda}{3\mu} P_2; P_3 = \frac{\lambda}{3\mu} * \frac{1}{2}\rho^2 P_0; P_3 = \frac{1}{3} * \frac{1}{2}\rho^3 P_0 \tag{43}$$

Equation 43 above could be expanded to better track the series.

$$P_3 = \frac{1}{3} * \frac{1}{2} * \frac{1}{1}\rho^3 P_0 \tag{44}$$

The service rate is 3μ going forward because $c = 3$ (in this example) there are only three servers.

$$\lambda P_3 = 3\mu P_4; P_4 = \frac{\lambda}{3\mu} P_1; P_4 = \frac{\lambda}{3\mu} * \frac{1}{3} * \frac{1}{2} * \rho^3 P_0; P_4 = \frac{1}{3} * \frac{1}{3} * \frac{1}{2}\rho^4 P_0; P_4 = \frac{1}{3^2} * \frac{1}{2} * \rho^4 P_0; \tag{45}$$

and the sum of all $P_i's$ equates to 1

$$\sum_{i=0}^{L} P_i = 1 \tag{46}$$

so

$$P_0+P_1+P_2+P_3+P_4 = 1; P_0+\frac{1}{1}*\rho P_0+\frac{1}{2}\rho^2 P_0+\frac{1}{3}*\frac{1}{2}*\frac{1}{1}\rho^3 P_0+\frac{1}{3^2}*\frac{1}{2}*\frac{1}{1}\rho^4 P_0 = 1; \tag{47}$$

$$P_0 * (1+\rho+\frac{1}{2}\rho^2+\frac{1}{3}*\frac{1}{2}*\rho^3+\frac{1}{3^2}*\frac{1}{2}*\rho^4) = 1 \tag{48}$$

solving for P_0,

$$P_0 = \frac{1}{(\sum_{i=0}^{c-1}\frac{1}{i!}*\rho^i)+(\sum_{i=c}^{L}\frac{1}{c!}*\frac{1}{c}^{(i-c)}*\rho^i)} \tag{49}$$

We can then calculate the state probabilities of the individual M/M/c/L (**noting that** $c = 1$ **in our case**) queues that constitute our tandem queuing model in Figure 3.4 as follows:

for $i < c$,

$$P_i = \frac{1}{i!}*\rho^i*P_0 \tag{410}$$

and for $i \geq c$

$$P_i = \frac{1}{c!}*\frac{1}{c}^{(i-c)}*\rho^i*P_0 \tag{411}$$

Using the state probabilities, P_i's for $i = 0, 1, 2, 3, ..., N$ and P_j's for $j = 0, 1, 2, 3, ..., L$, we can obtain the state probabilities for our two-dimensional Markov process, $P_{i,j}$'s, by cross multiplying the state probabilities of the up-link and relay stages such that $P_{i,j} = P_i * P_j$ for $i = 0, 1, 2, 3, ..., N$ and $j = 0, 1, 2, 3, ..., L$.

4.1.1 Accounting for relaying and feedback

Lastly, we need our derivation to account for the forwarding and feedback probabilities (θ_1 and θ_2). The proposed queuing model in Figure 3.4 is essentially constructed on the blueprint of the two-stage queuing model put forward as a model for the heterogeneous network mentioned in Figure 2.4 [12] by Yaqoob et al. with the exception

of the single channels used in both stages our case.

We can therefore adapt the use of an effective arrival rate (denoted as λ_e) from [12] similarly maintained below $c\mu_1$ (i.e., μ_1 since $c = 1$) for the system to be at stable state; in lieu of the λ value used in Equations 41 to 411.

Another imperative point to note is that we will apply the use of λ_e in calculating the initial P_i and P_j state probabilities using Equations (410) and (411) to propagate the effect of θ_1 and θ_2 throughout the queue contrary to its application to the first stage only in [12] in the product form solution presented to solve the queuing system by Yaqoob et al.

The derivation of λ_e for the introduced tandem system comprising two M/M/c/L queues (where $c = 1$) follows the iterative logic below

Table 4.1 Derivation of effective arrival rate, λ_e

Iteration	Feedback	Effective arrival rate, λ_e
0		λ
1	$\lambda\theta$	$\lambda + \lambda\theta = \lambda(1+\theta)$
2	$\lambda(1+\theta)\theta$	$\lambda + \lambda\theta + \lambda\theta^2 = \lambda(1+\theta+\theta^2)$
3	$\lambda(1+\theta+\theta^2)\theta$	$\lambda + \lambda\theta + \lambda\theta^2 + \theta^3 = \lambda(1+\theta+\theta^2+\theta^3)$
.	.	.
.	.	.
.	.	.
i	$\lambda(1+\theta+\theta^2+...+\theta^i)$	$\lambda \sum_{n=0}^{i} \theta^n$

From the above, we can arrive at the conclusion;

$$\lambda_e = \lambda \sum_{n=0}^{\infty} \theta^n; \tag{412}$$

which we can then express as,

$$\lambda_e = \lambda * \frac{1}{1-\theta} = \frac{\lambda}{1-\theta} \tag{413}$$

Expanding this notation for the two-stage queuing for which we are modelling, we

can express the effect of θ_1 and θ_2 as;

$$\lambda_e = \lambda_1 + \lambda_1\theta_1\theta_2 + \lambda_2\theta_2... \tag{414}$$

$$\lambda_e = \lambda_1 + \lambda_1\theta_1\theta_2 + \lambda_1(\theta_1\theta_2)^2 + \lambda_2\theta_1\theta_2^2 + \lambda_2\theta_2... \tag{415}$$

$$\lambda_e = \lambda_1 + \lambda_1\theta_1\theta_2 + \lambda_1(\theta_1\theta_2)^2 + \lambda_1(\theta_1\theta_2)^3 + \lambda_2\theta_1^2\theta_2^3 + \lambda_2\theta_1\theta_2^2 + \lambda_2\theta_2... \tag{416}$$

$$\lambda_e = \lambda_1 \sum_{n=0}^{i}(\theta_1\theta_2)^n + \lambda_2\theta_2 \sum_{n=i}^{0}(\theta_1\theta_2)^n;\ \lambda_e = \lambda_1 \sum_{n=0}^{l}(\theta_1\theta_2)^n + \lambda_2\theta_2 \sum_{i=n}^{0}(\theta_1\theta_2)^n \tag{417}$$

since the above series notation can be expressed as

$$\sum_{n=0}^{L}(\theta_1\theta_2)^n = \frac{1}{1-\theta_1\theta_2}$$

, λ_e can ultimately be contracted into the formula;

$$\lambda_e = \frac{\lambda_1 + \lambda_2\theta_2}{1-\theta_1\theta_2} \tag{418}$$

This hitherto derived effective arrival rate, λ_e, is the value used to calculate the initial state probabilities, P_i's and P_j's (of the individual M/M/1/L queues comprising our two-stage model) required for step (i) mentioned in the description of the iterative solution at the start of Chapter 4.

We now have the parameters required to set up the initial conditions that will kick off our iterative model.

4.2 Performance Measures

The performance measures that are tracked to verify the validity of the proposed queuing model in this study are the mean queue length, throughput and response time. We shall use the following Equations (419) to (424) gleaned from [3] by Ever et al. to obtain the analytical results of the above queuing performance from the state probabilities, $P_{i,j}$'s, at which the model will have converged at the end of the iterative run.

NB: Recalling that the queue capacity limit of the UAVRN stage of the queue is N and that of the BS stage is L;

Mean queue length at the UAVRN stage,

$$MQL_{UAVRN} = \sum_{j=0}^{L} j \sum_{i=0}^{N} P_{i,j} \tag{419}$$

Mean queue length at the BS stage,

$$MQL_{BS} = \sum_{i=0}^{N} i \sum_{j=0}^{L} P_{i,j} \tag{420}$$

Throughput at the UAVRN stage,

$$\gamma_1 = \mu_1(1 - \sum_{j=0}^{L} P_{0,j}) \tag{421}$$

Throughput at the BS stage,

$$\gamma_2 = \mu_2(1 - \sum_{i=0}^{N} P_{i,0}) \tag{422}$$

Response time at the UAVRN stage,

$$RT_{UAVRN} = \frac{MQL_{UAVRN}}{\gamma_1} \tag{423}$$

Response time at the BS stage,

$$RT_{BS} = \frac{MQL_{BS}}{\gamma_2} \tag{424}$$

4.3 Convergence

Following step (iv) of the iterative method, the next phase of the iterative solution simply involves running the loop that is used to assign the state probabilities, $P_{i,j}$'s, using the Equations (31) to (39) with the term $P_{i,j}$ as the subject of the formulae.

As explained in 3.2 the aforementioned balance equations cater for all the possible regions in the 2d transition lattice in Figure 3.5 that results from the implementation of the proposed two-stage queue.

The number of iterations required governed by the formulae used to check for convergence after each iteration; ($|MQL_{old} - MQL_{new}| < \epsilon$). It would be prudent to note that the stability of the system i.e., utilisation (denoted as $u = 1 - P_0$, where P_0 is the idle probability of the individual queue - either the up-link or the relay stage) $\leq$ 1 and the sum of all state probabilities, $P_{i,j}$'s $\approx$ 1.0, is maintained throughout the run of the analytical model.

4.4 The Simulation Program

The **in-house** simulation program used to validate the results from the analytical model is similar to the ones used in works such as [12, 3, 36, 37]. Mathematically, the in-house simulation model follows the same exponential distribution of inter-arrival and service times for both stages one and two. A discrete-event simulation program is one which can used to model real world systems that can be decomposed into a set

of logically separate processes that autonomously progress through time. Each event occurs on a specific process, and is assigned a logical time (a timestamp). This approach avails the ability to change simulation inputs and observe the resulting outputs can produce valuable insight into which variables are the most important and into how variables interact [37]. This plays right into our scenario as we seek to investigate the effect of a select set of system parameters on specific performance measures of our queuing system. Written in C++, the discrete-event simulation program mimics the behaviour of the disaster recovery scenario and tracks the packet lifetimes from entry, to relaying to feedback and then exit. The program receives an input text file containing the system parameters (explored below in Section 5.1) and gives an output text file containing the performance measures being investigated (mean queue length, throughput and response time) for both stages one and two as well as the execution time of the run for the given set of parameters.

CHAPTER 5

RESULTS AND DISCUSSIONS

In this section, the results obtained from the iterative analytical solution elaborated in Chapter 4 are contrasted with the simulation results. Similar to the simulation model described (4.4), the analytical model was implemented in C++. Discussion of the trends observed in the results obtained and accompanying explanations follow each set of graphs. A comment on the iterative solution implemented is also covered.

5.1 System Parameters

In line with proposed models used for heterogeneous networks, the radius of the cell is taken to be 1000 metres [38] and the line-of-sight range/radius of coverage of the UAV-RN is taken to be that of a standard disaster management/search and rescue drone at 1000 metres [39]. The maximum velocity, V_{max}, of the Intel Aero Ready-to-Fly drone is taken to be $15m/s$ from [40]. However, we are making the assumption that the continuous and most times redundant coverage provided as the drone traverses the cell border, as in Figure 3.6, coupled with the lightweight nature of the SOS packets negates the explicit effect of the UAV-RN's velocity on the arrival and service rates and hence the performance measures of the queuing model.

Indeed, taking an example of a scenario where the probability of relaying from stage one to stage two, θ_1, is 0.6, the probability of a miss (due to line-of-sight issues, poor physical conditions caused by the ongoing disaster or its aftermath, signal attenuation due to the UAV-RN having to fly at a higher altitude than the optimum, etc) would be $1 - \theta_1$ i.e., 0.4. Each of the ground devices is broadcasting its SOS packet in a heart-beat rhythm every second (in this example) as indicated in the assumptions discussed in 3.1, with the UAV traversing the sub-cell (ideally the $1km$ length of the side of the macro-cell as seen in Figure 3.6) at a velocity, V_{max}, of $15m/s$ consequently provid-

ing continuous coverage to the stranded devices. The UAV would provide coverage for up to $66.667s$ thus still able to pick up the SOS packets. This follows the fact that the probability that all twenty tries (one for each second) are misses exponentially decreases towards a negligible value with each broadcast attempt (in this case, probability of all twenty broadcasts being misses would be 0.4^{20}). We can therefore safely assert that the likelihood of an SOS packet not being received during a traversal is down to factors not to do with the operational parameters of the UAV-RN, thus outside of our control as pertains to this study.

The physical layer parameters of the drone are incorporated in the system parameters, especially the UAV-RN service rate, μ_1, specified throughout this chapter.

Seeing as existing literature is limited in queue modelling in this context, most of the queuing parameters used in this study have been selected following composite studies that we have used to build the proposed solution [3, 12, 13]. This is, of course, provided that the system stability is maintained in line with the mathematical presuppositions of Markov models.

Predicated upon the assumption that the proposed framework would be a fail-safe and not dependent on the current channel infrastructure, the channel capacities of both the UAV-RN and the base station are 1; with the latter being an emergency channel that is otherwise unused. We can afford to have an unused BS channel because even at high queue capacities, the size of the SOS packets (discussed in 3.1) being received are extremely lightweight in comparison to standard data packets. It is hence expected that its bandwidth would be significantly lower (albeit consistent). To that effect, the overhead cost of maintaining this channel when it is not being used would be negligible to the performance of the BS link during normal operations.

The **standard** queue capacity of the emergency channel at the operational base station as well as that of the UAV-RN is 1500 packets [41]. The **standard** arrival rate at the UAV-RN stage, λ_1 is 500 packets per second while that at the emergency channel at the operational BS, λ_2, is 500 packets per second. The **standard** service rate at the UAV-RN stage, μ_1, is 2000 packets per second while that at the emergency channel at the operational BS, μ_2, is 1000 packets per second. In the next sub-section, varying

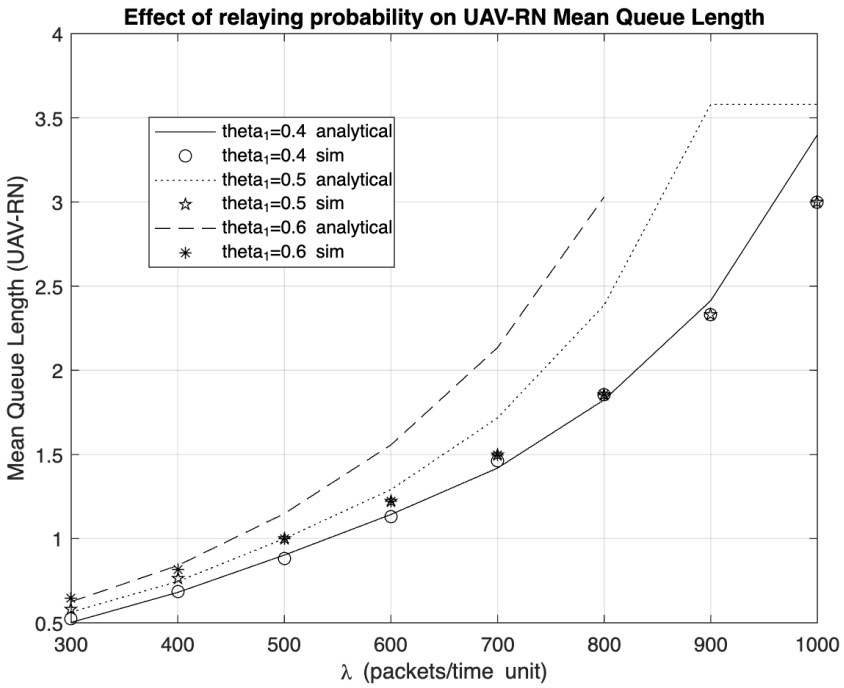

Figure 5.1 Effect of θ_1 on UAV-RN Mean Queue Length

relaying probabilities (θ's), arrival rates (λ's) and service rates (μ's) have been used in the evaluation of the iterative model within the bounds of system stability.

5.2 Numerical Results

The graphs are labelled and separated by order of performance measure (mean queue length, throughput then response time) for ease of reading as well as comparison. Accompanying discussions are provided to aid in comprehension.

The set of graphs below (Figures 5.1 to 5.12) shows the effect of relaying probability, θ_1, and feedback probability, θ_2, on the selected performance measures - mean queue length, throughput and response time. To investigate the effect of θ_1, we have maintained the standard system parameters specified in the previous sub-section (5.1) while increasing the value of λ_1 until the system is no longer stable.

Concerning the mean queue length at the UAV-RN stage, denoted as MQL_{UAVRN}, a vital trend to note would be the increase in mean queue length values with increase in λ_1. For both the simulation and analytical model results, the mean queue length in-

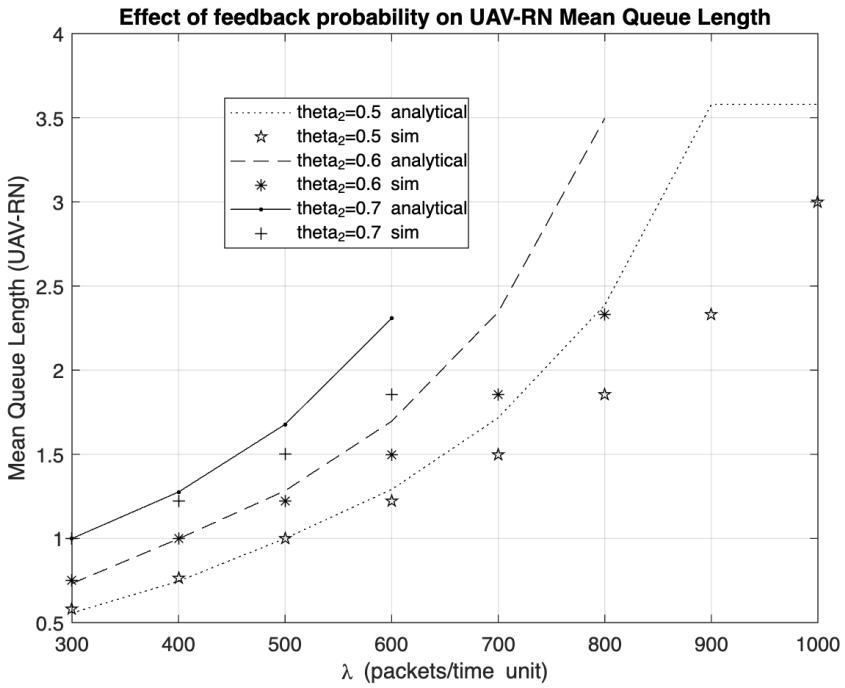

Figure 5.2 Effect of θ_2 on UAV-RN Mean Queue Length

creases steadily with each increasing interval of λ_1 but is maintained at a significantly low value. This is to be expected due to the high service rate at the UAVRN stage, μ_1, capped at a constant value of 2000 packets per second.

Moreover, from the graphs contrasting MQL_{UAVRN} results for the analytical and simulation models (Figure 5.1 for θ_1; Figure 5.2 for θ_2), we can identify the jump point of each of the performance measures for each θ_1 value. The "jump point" (to which we have also referred interchangeably as **critical** λ_1) refers to the λ_1 value at which the mean queue length of the UAV-RN and/or the BS stage jumps to a value very close to the respective queue capacity limit (N or L respectively) thus causing the system to approach instability. In the graphs that track the effect of θ_1 on the mean queue length of the UAVRN stage, this point is distinctly characterised by the divergence point of the simulation and analytical model plots contrasted on the plane. At this λ_1 value, the mean queue length increases significantly to a value approaching the maximum queue length, either at the first or stage or both, thus indicating that the system is approaching instability. The discrepancy between mean queue length values (of stage one) of the simulation and analytical models likewise decreases steadily as λ_1 approaches this ***critical*** λ_1 value. The plots then diverge as λ_1 increases afterwards

as the MQL values of the second stage nearing the queue capacity limit, L, with the system approaching instability. The convergence and divergence increases with increasing θ_1 values. The latter is an effect of more incoming packets per unit time as is expected by increasing λ_1. For the range of stable λ_1 values, the maximum discrepancy between the analytical and simulation values exhibited was 4.0313%. Upon further observation, it is also notable that the λ_1 value at which the jump occurs decreases with increasing θ_1 value; at 600 packets per second when $\theta_1 = 0.4$, 500 packets per second when $\theta_1 = 0.5$, 400 packets per second when $\theta_1 = 0.6$.

For the chosen range of θ_1 values and the range of λ_1, the MQL of stage one never approaches the queue capacity limit, N, owing to the high service rate, μ_1, constant at 2000 packets per second in this run. Stage two on the other hand always reaches queue capacity before stage one due to the lower service rate capped at 1000 packets per second. In fact, the critical λ_1 value explored throughout this section is solely determined by the sudden increase of stage two MQL values.

With regard to feedback probability, θ_2, the effect on the mean queue length is similar. In Figure 5.2, the critical λ_1 value for the respective θ_2 value is characterised by the point in the plot where the simulation and analytical plots begin to diverge. For the range of stable λ_1 values, the maximum discrepancy between the analytical and simulation values exhibited was 3.7391%. As the graph depicts, the divergence exhibited in the simulation and analytical model results being compared is due to the critical λ_1 having been reached with the MQL of the second stage suddenly shooting up to values much closer to the BS stage queue capacity limit, L, and the system approaches instability. With relaying probability, θ_1, maintained at 0.5 while investigating the effect of θ_2, we can ascertain that the critical λ_1's achieved are identical as those recorded when investigating the effect of θ_1. This could be attributed to the value of θ_1 chosen. In fact, the rationale for selecting θ_1 as 0.5 comes from the results obtained from investigating the effect of θ_1 (explained above). From the results, the MQL value obtained at the second stage, 750, when λ_1 is 500 packets per second, is such that it is not too low that the system is underutilised but not too high that we risk the system becoming unstable. To this effect, we can circle back to the **standard** parameters selected towards the end of the "System Parameters" section (5.1) and

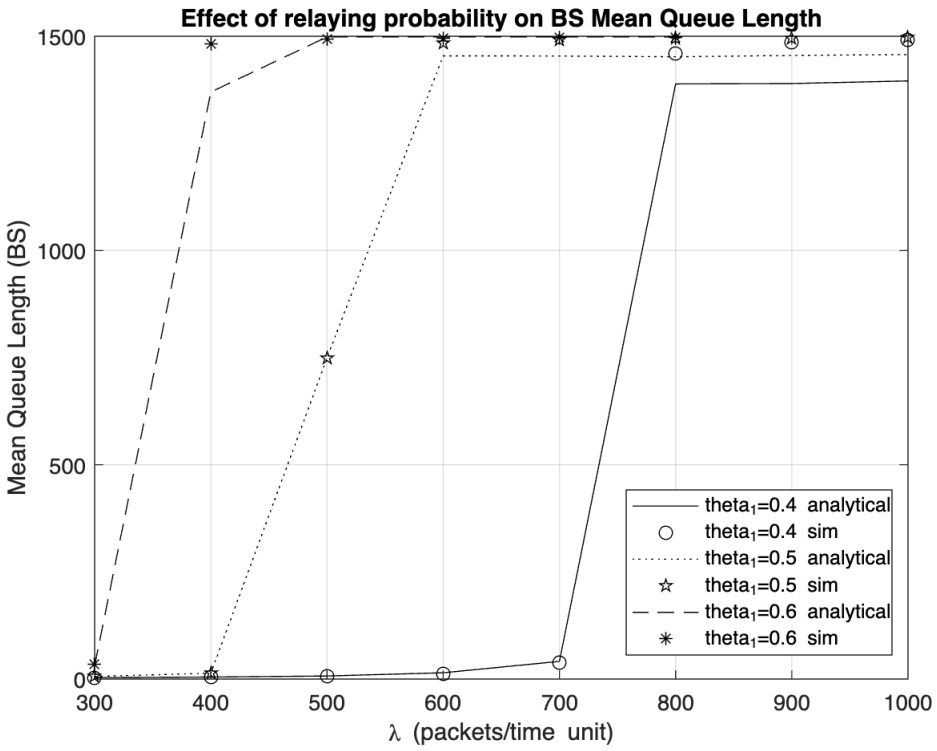

Figure 5.3 Effect of θ_1 on BS Mean Queue Length

confirm that indeed they are ideal.

With reference to the mean queue length at the BS stage, denoted as MQL_{BS}, the trends for the mean queue length results are much more predictable. Similar to the behavior of the results obtained for the effect of vertical upward handover on femtocell mean queue length in [12], the graphs (Figure 5.3 for θ_1; Figure 5.4 for θ_2) unmistakably depict the rising MQL value with increasing λ_1 intervals as well as the sudden jump point of each θ_1 after which the mean queue length value plateaus as it approaches the queue capacity limit, L, and the system becomes unstable. In line with the findings ascertained from the set of graphs showing the effect of θ_1 on MQL of the UAV-RN stage, we can also see the fact that the aforementioned critical λ_1 i.e., the jump point occurs sooner when the relaying probability, θ_1, is higher. In this run, the maximum discrepancy between the analytical and simulation results was 4.0212%.

Akin to the effect of θ_1, the notable effect of feedback probability, θ_2 is that the critical λ_1 value is reached much faster with increasing θ_2. This is best exhibited by the behaviour of the system when θ_2 is 0.7 where the system almost instantly becomes

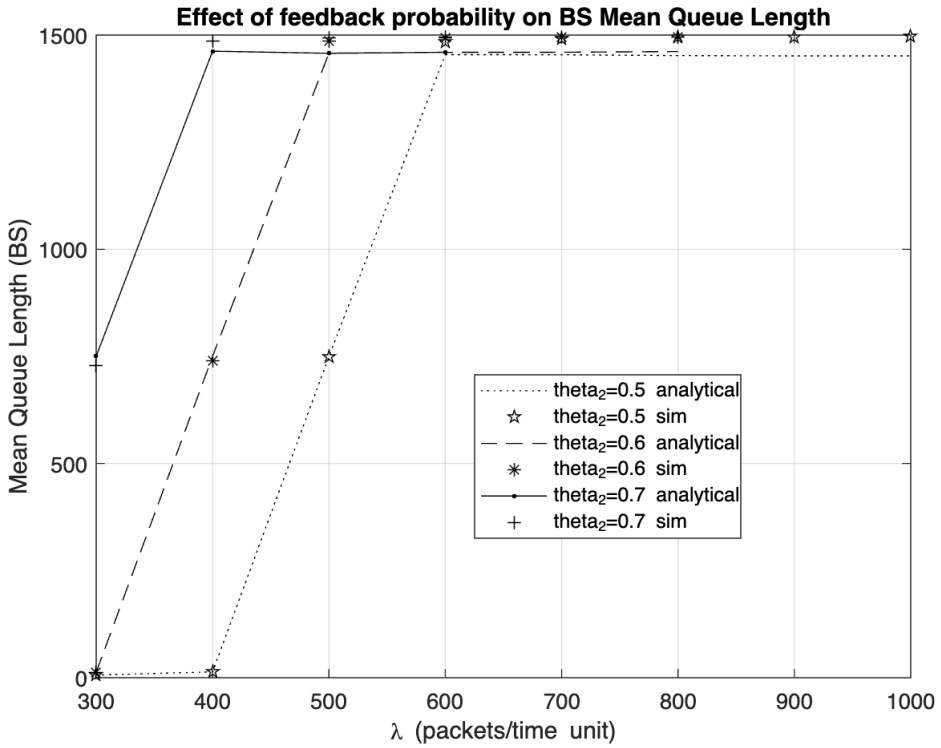

Figure 5.4 Effect of θ_2 on BS Mean Queue Length

unstable. This further justifies the use of the standard value of 0.5 for our relaying and feedback probabilities. In this run, the maximum discrepancy between the analytical and simulation results was 2.6687%.

Regarding throughput at the UAV-RN stage, denoted as γ_1, as per Figure 5.5 for θ_1 and Figure 5.6 for θ_2, the simulation and analytical model values of the throughput at the first stage increase with increasing λ_1 and then diverge as λ_1 increases after the critical λ_1 has been reached. This is similar to the trend of MQL_{UAVRN}. We can also identify the critical λ_1 value at which the simulation and analytical models' values diverge. Up until the critical λ_1, i.e., while the system is stable, the results obtained from the analytical model are within the targeted 5% confidence interval with the maximum discrepancy being 3.78261% under stable conditions. This discrepancy value can be improved but that would require increasing the number iterations which in turn would increase the execution time of the analytical model. The aforementioned divergence is also attributed to the MQL at the BS stage, MQL_{BS} having shot up to a value approaching the queue limit at the BS stage as the system approaches instability. The throughput values obtained at this UAV-RN stage are significantly

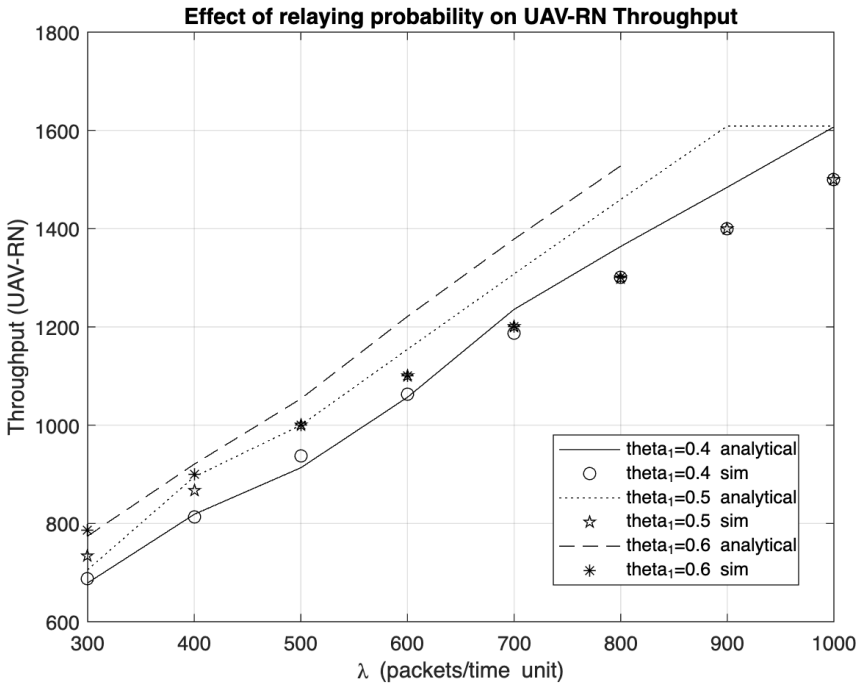

Figure 5.5 Effect of θ_1 on UAV-RN Throughput

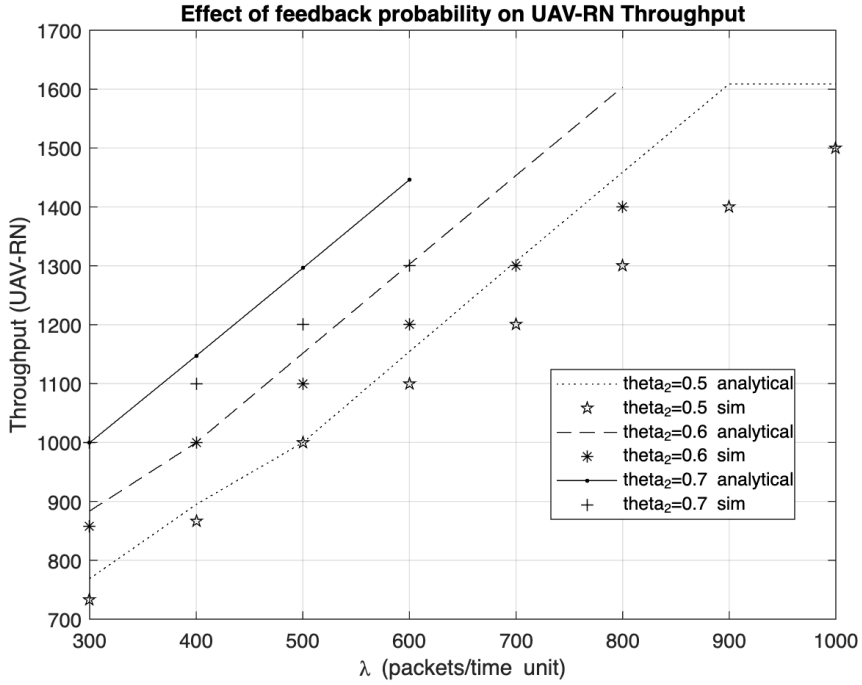

Figure 5.6 Effect of θ_2 on UAV-RN Throughput

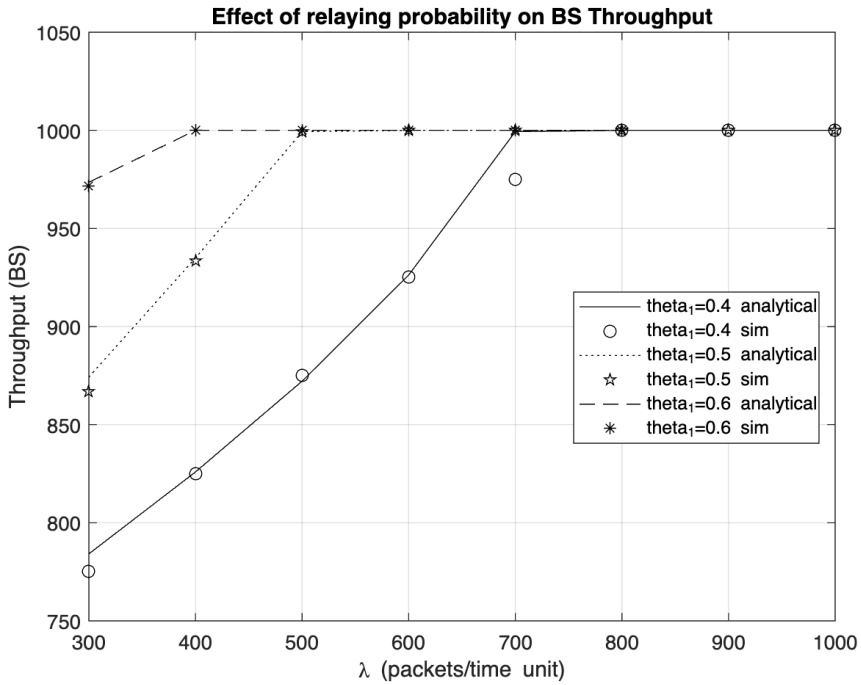

Figure 5.7 Effect of θ_1 on BS Throughput

low also due to the very high service rate, μ_1 capped at 2000 packets per second. The same observation can be made for the effect of θ_2; with the additional observation that the high throughput values which increase steadily toward the maximum queue capacity, N for the UAV-RN stage and L for the BS stage are due to the relatively high service rates and increasing incoming packets into the system governed by λ_1.

On throughput at the BS stage, denoted as γ_2, as shown in the set of graphs (Figure 5.7 for θ_1 and Figure 5.8 for θ_2), the behaviour of the second stage throughput is consistent through changing θ_1 values for both the simulation and analytical model results. The throughput value increases steadily with increased λ_1 and plateaus after λ_1 exceeds the critical λ_1 values at which the MQL of stage two jumps to values approaching the queue limit, L, as the system approaches instability. This observed increase in throughput can be attributed to increased packets through the UAVRN due to steadily increasing incoming packets per unit of time. Similar to θ_1, the effect of θ_2 on the throughput value of the second stage is such that the plateau point occurs earlier with higher θ values. This plateau point is consistent with the jump point exhibited in the graphs showing the effect of θ_1 and θ_2 on the mean queue length.

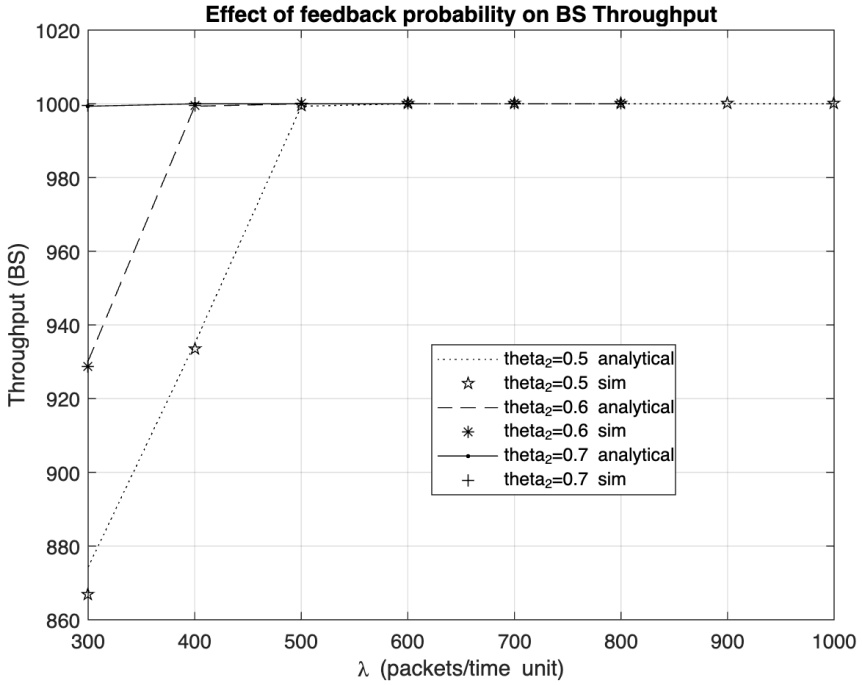

Figure 5.8 Effect of θ_2 on BS Throughput

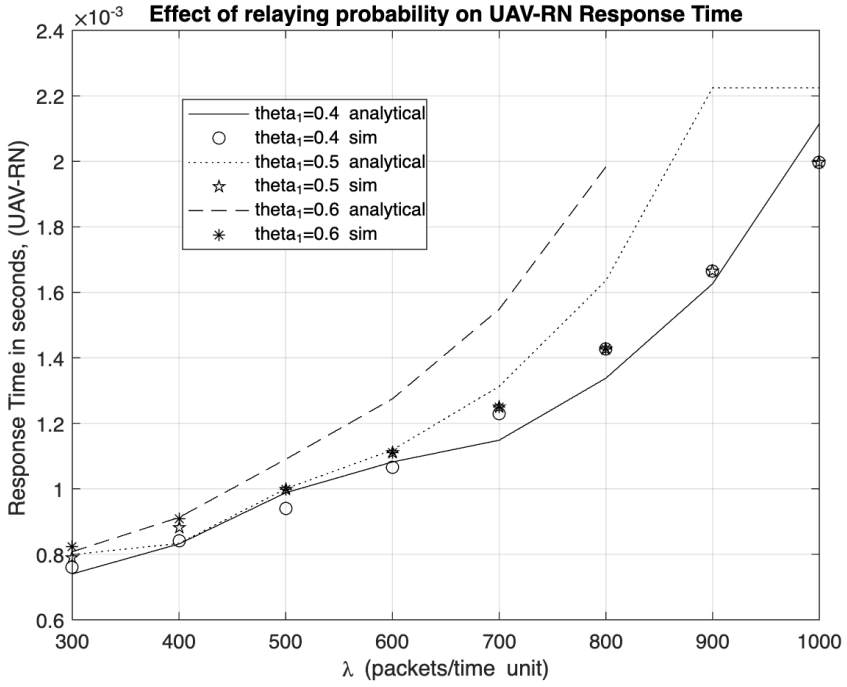

Figure 5.9 Effect of θ_1 on UAV-RN Response Time (in seconds)

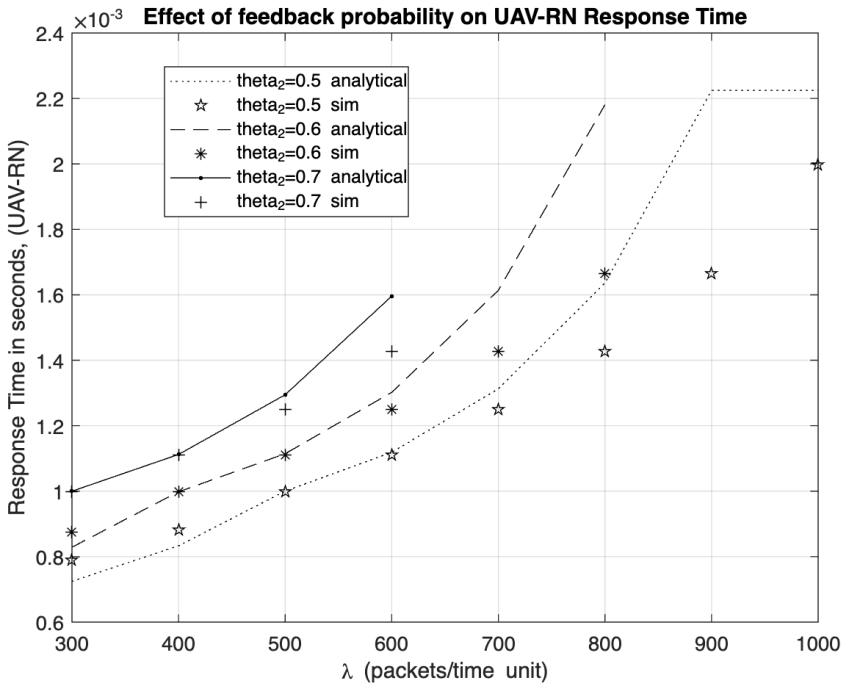

Figure 5.10 Effect of θ_2 on UAV-RN Response Time (in seconds)

About the behaviour of response time at the UAV-RN stage, denoted as RT_{UAVRN}, despite increasing steadily with increasing λ_1 values i.e., more incoming packets per unit of time, the response times for the first stage are very low due to the high service rate. It is also notable from the [relevant] graphs (Figure 5.9 for θ_1 and Figure 5.10 for θ_2) that, as expected, the behavior of the response time mimics that of the mean queue length almost to a tee, indicating up to the critical λ_1 after which the MQL of the second stage shoots to values approaching the queue capacity limit as the system approaches instability.

The effect of both θ_1 and θ_2 on the response time of stage one is similar as per the graphs in Figures 5.9 and 5.10; with the simulation and analytical plot points diverging after the critical λ_1 for each investigated θ value. The divergence exhibited is due to the system approaching instability owing to the MQL of the second stage having drastically increased to values very close to the maximum queue capacity. Similar to the graphs depicting the behaviour of mean queue length in response to θ_1 and θ_2 for the UAV-RN stage (Figures 5.1 and 5.2), we are able to predict this critical λ_1 within the acceptable 5% error margin in keeping with the confidence interval of the simulation program [12].

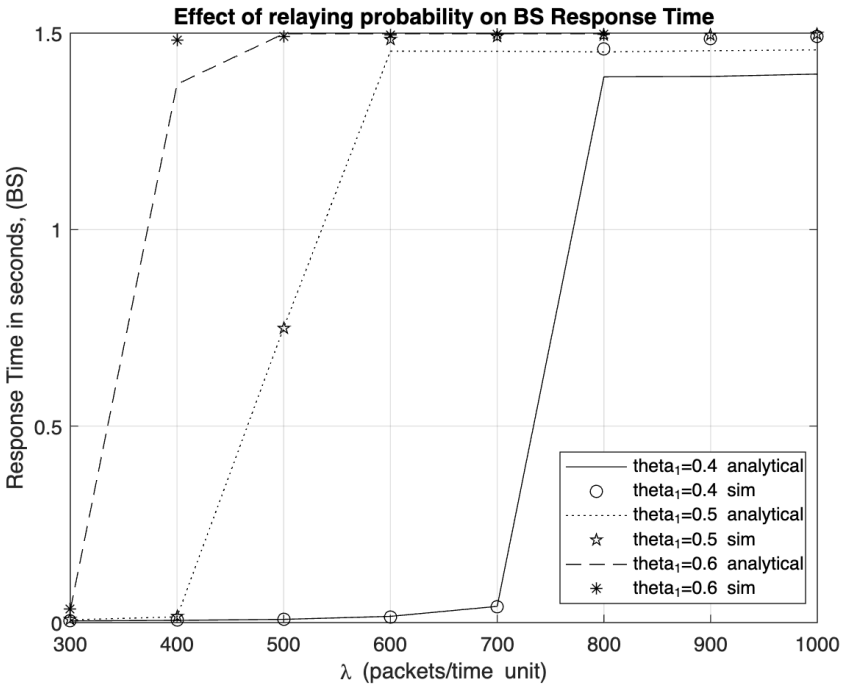

Figure 5.11 Effect of θ_1 on BS Response Time (in seconds)

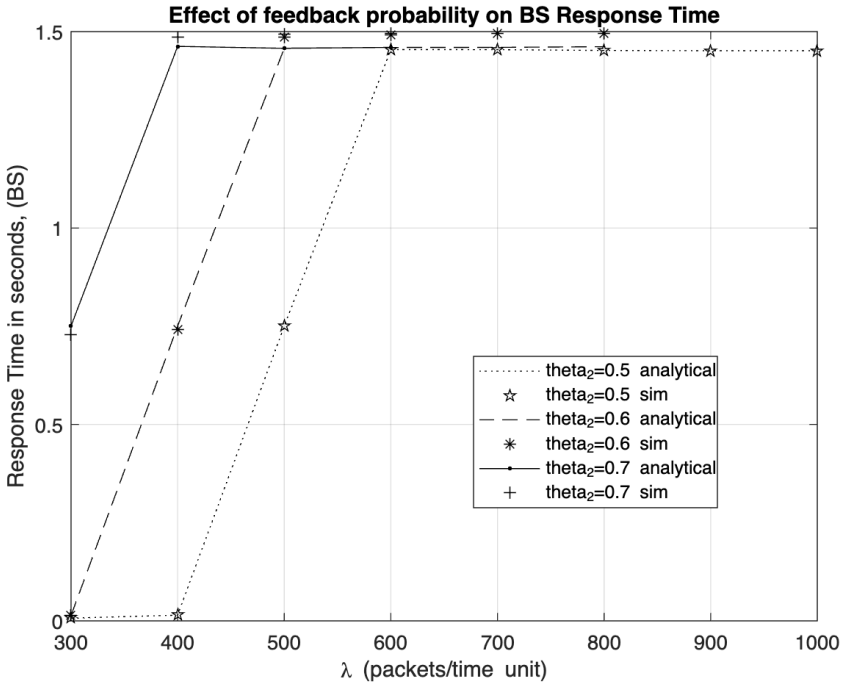

Figure 5.12 Effect of θ_2 on BS Response Time (in seconds)

With respect to the response time at BS stage, denoted as RT_{BS}, similar to the first stage, the response time increases steadily with increasing incoming packets at stage one with the critical λ_1 occurring sooner due to more incoming packets per unit of time. This is attributed to the fact that with higher θ_1 values (Figure 5.11 for θ_1 and Figure 5.12 for θ_2), more packets are being forwarded to the second stage and since the feedback probability, θ_2, is being held constant at 0.5, more packets would be in turn be fed back to the first stage and so on and so forth, causing the system to approach instability much sooner i.e., packets getting accumulated in the system and increasing response time. The case is the same for increasing θ_2. Increasing θ_2 while maintaining θ_1 at 0.5 translates to more packets being fed back to stage one resulting in the system accumulating packets and the relative increase in the response time.

On the range of acceptable arrival rates at the UAV-RN stage, denoted as λ_1, the common trend exhibited across the set of graphs depicting the effect of varying different parameters pertains to the range of acceptable primary arrival rates at the UAV-RN stage, λ_1. An increase in the value of relaying probability, θ_1 decreases the acceptable range of primary arrival rates, λ_1. This is expected due to more packets being relayed to the second stage which translates into the second stage reaching instability at a much lower λ_1 value. For instance, we can see that the range of arrival rates extends to 1000 packets per second, after which the system becomes unstable when $\theta_1 = 0.4$. This limit is maintained at 1000 packets per second when $\theta_1 = 0.5$ but decreases to 800 packets per second when $\theta_1 = 0.6$.

The observed trend in the effect of θ_1 is due to the steady increase in the number of packets being forwarded to the second stage, and with the feedback probability, θ_2 kept constant value of 0.5, this translates to more packets being feedback to the UAV-RN stage, thus filling up the queue much sooner i.e., at lower values of lambda with each higher value of θ_1.

Additionally, the subset of graphs showing the behavior of the second (BS) stage indicate that the system almost immediately becomes unstable when θ_1 and θ_2 are 0.7. This is in line with our previous observation of the value of critical λ_1 decreasing steadily with increasing θ_1 and indeed θ_2 values. We can therefore rule out the use of

0.7 as the relaying probability.

As for the effect of θ_2, increasing the feedback probability increases the amount of packets forwarded to the BS stage even when θ_1 is kept constant. This in turns causes the second stage to get filled up much quicker especially owing to the lower service rate, μ_2 capped at 1000 packets per second.

On the whole, the trend of results for both the UAV-RN and BS stages are pretty similar for the effects of relaying probability, θ_1, and feedback probability, θ_2. The rationale behind the use of a lower standard BS service rate (1000 packets/second) in comparison to the standard service rate at the UAV-RN stage ((2000 packets/second) is because we wanted to showcase the behaviour of the system as it approaches the critical λ_1 as well as afterwards when the system approaches instability. The resulting effect produces the initial gradual increase as incoming number of packets per unit of time increases towards the critical rate, subsequent abrupt jump at the critical λ_1 and eventual plateau as the MQL of the BS stage of the queue hits a value very close to the queue limit, L. This also holds for the general trend of the response time. It is also evident that the discrepancy between the service rates allows for the UAV-RN stage to never be overwhelmed since the BS stage governs whether the system is stable or not. The UAV-RN queue limit, N, is hence never reached. At least not with the system operating at the given parameters.

The service rates, μ_1 and μ_2, are still however maintained at realistic values throughout. Consider a scenario that calls for incorporating the packet size in determining the service rates. Recalling that the approximate size of an SOS packets in our proposed model is 35 bytes, a μ_1 value of 2000 packets per second would translate to a data rate of 0.56 Mbps. This low data rate requirement is very friendly on the throughput and energy consumption needs of the UAV-RN.

For Table 5.1, taking λ_1 = 500 packets/s, λ_2 = 500 packets/s, μ_2 = 1000 packets/s, θ_1 = 0.5 and θ_2 = 0.5.

Concerning the range of acceptable UAV-RN service rates, denoted as μ_1, we can observe from Table 5.1 the effect of varying the relay node's service rate. While

Table 5.1 Effect of [stable range of] UAV-RN service rates, μ_1, on Mean Queue Length.

μ_1	MQL_{UAVRN}			MQL_{BS}		
	Iterative	**Simulation**	**% discrepancy**	**Iterative**	**Simulation**	**% discrepancy**
1000	750	722.3676	3.825254621	750	717.3996	4.544245634
1100	10	9.9396	0.017913208	750	745.1917	0.645243365
1200	5	4.9855	0.016892853	750	723.9994	3.59124607
1300	3.3333	3.3254	0.018793531	750	745.9461	0.543457496
1400	2.5	2.4947	0.017092921	750	743.785	0.83559093
1500	2	1.9962	0.023135351	750	722.9704	3.73868695
1600	1.66667	1.6639	0.01640269	750	747.1679	0.379044656
1700	1.42857	1.4264	0.020054021	750	735.3434	1.99316401
1800	1.25	1.2484	0.016932867	750	739.9751	1.354761802
1900	1.11111	1.1095	0.020734298	750	733.5722	2.239425104
2000	1	0.999	0.018673486	750	730.4561	2.675574891

MQL_{UAVRN} decreases with increasing service rate at the UAV-RN due to more packets being served per unit time, MQL_{BS} oscillates around the 750 mark (that was discussed under the effect of relaying probability, θ_1, and feedback probability, θ_2, on the MQL) identified as being the point at which the system's resources are being optimised given the standard parameters. The standard service rate specified for the UAV-RN is 2000 packets per second. With the 35-byte large SOS packet discussed throughout this study, this translates to 0.6 Mbps which for a channel that is expected to be operating on 4G, 5G or some other future generation wireless network infrastructure, is a relatively low ask. Thus, the channel is almost guaranteed to never be overwhelmed provided the parameters are maintained within those prescribed by the findings of this study. To this effect, expecting the framework to facilitate this maximum service rate at the UAV-RN (albeit it may be viewed as being quite high), would not be a significant impediment as it improves the efficiency by a great deal.

To track the effect of the BS service rate, μ_2, on the MQL (Table 5.2), throughput and response time (Table 5.4), the following system parameters used: $\lambda_1 = 500$, $\mu_1 = 1000$, $\lambda_2 = 500$, $\theta_1 = 0.5$, $\theta_2 = 0.5$, $N = 1500$, $L = 1500$.

In this case depicted in Table 5.2, for the range μ_2 values for which both stages of the system are stable, the MQL of the BS decreases gradually with increase in service

Table 5.2 Effect of [stable range of] BS service rates, μ_2, on Mean Queue Length.

μ_2	MQL_{UAVRN}			MQL_{BS}		
	Iterative	**Simulation**	**% discrepancy**	**Iterative**	**Simulation**	**% discrepancy**
1200	750	746.3011	0.495631053	5	4.997	0.645243365
1400	750	731.7714	2.491023836	2.5	2.4972	3.59124607
1600	750	738.2025	1.598138722	1.66667	1.6658	0.543457496
1800	750	734.7447	2.076272207	1.25	1.2489	0.83559093
2000	750	747.6664	0.023135351	1	0.9995	3.73868695
2200	750	748.6592	0.01640269	0.83333	0.8329	0.379044656
2400	750	743.0074	0.020054021	0.714286	0.7139	1.99316401

rate as expected due to more packets leaving this stage per time unit. The MQL at stage one is, however, somewhat oscillates at 750 packets. Similar to the effect of μ_1 on the MQL explored in Table 5.1, this could be attributed to chosen θ_1 and θ_2 values, both capped at 0.5.

Pertaining throughput, increasing the service rates at the UAV-RN, μ_1, as well as the BS, μ_2, has little to no effect. This is because the margins of change in the mean queue length seen in Table 5.1 and 5.2 are almost negligible relative to the amount of packets needed for the system to approach instability.

Table 5.3 Effect of [stable range of] UAV-RN service rates, μ_1, on Response Time (in seconds).

μ_1	$Response\ Time_{UAVRN}$			$Response\ Time_{BS}$		
	Iterative	**Simulation**	**% discrepancy**	**Iterative**	**Simulation**	**% discrepancy**
1000	0.750499833	0.722874552	3.821587147	0.750499833	0.71797671	4.529829836
1100	0.01	0.009941381	0.589651495	0.750499833	0.74556948	0.661286837
1200	0.005	0.004986342	0.273904323	0.750499833	0.724376873	3.606266445
1300	0.0033333	0.003326025	0.218730767	0.750499833	0.746309254	0.561507014
1400	0.0025	0.002495126	0.195324087	0.750499833	0.744135637	0.855246794
1500	0.002	0.001996662	0.167187657	0.750499833	0.723343501	3.754278885
1600	0.00166667	0.001664173	0.150049049	0.750499833	0.747538904	0.396090333
1700	0.00142857	0.001426686	0.132050737	0.750499833	0.735717439	2.009248845
1800	0.00125	0.001248611	0.111212352	0.750499833	0.740333199	1.373251089
1900	0.00111111	0.00110973	0.124350329	0.750499833	0.733962742	2.253124086
2000	0.001	0.000999187	0.081411411	0.750499833	0.730853904	2.688078836

It then follows that the response times gleaned from the data above using Equations 423 and 424 would produce a downward trend for the UAV-RN stage, as in Table 5.3,

Table 5.4 Effect of [stable range of] BS service rates, μ_2, on Response Time (in seconds).

μ_2	$Response\ Time_{UAVRN}$			$Response\ Time_{BS}$		
	Iterative	**Simulation**	**% discrepancy**	**Iterative**	**Simulation**	**% discrepancy**
1200	0.750499833	0.746678172	0.511821632	0.005	0.004997895	0.042125275
1400	0.750499833	0.732152046	2.506007754	0.0025	0.002497693	0.0923834695
1600	0.750499833	0.738545111	1.61868539	0.00166667	0.001666035	0.038129799
1800	0.750499833	0.735137484	2.089724612	0.00125	0.001249219	0.062505004
2000	0.750499833	0.748043713	0.328339052	0.001	0.000999665	0.033536768
2200	0.750499833	0.749049755	0.193589056	0.000833066	0.747538904	0.031646536
2400	0.750499833	0.743401923	0.954787614	0.000714036	0.735717439	0.035058924

Table 5.5 Contrasting CPU run times (in seconds) for testing the range of stable μ_1.

μ_1	$Run\ Time_{Iterative}$	$Run\ Time_{Simulation}$
700	0.386391	239.22
800	0.395816	250.77
900	0.388788	259.79
1000	0.385237	317.49
1100	0.386434	253.03
1200	0.366956	252.93
1300	0.385981	252.74
1400	0.394706	252.07
1500	0.387878	250.98
1600	0.353647	249.73
1700	0.459266	250.64
1800	0.476825	249.37
1900	0.438693	247.89
2000	0.346084	247.93

due to more packets being serviced per unit of time and a plateauing trend at the BS stage due to the relatively constant mean queue length and throughput values in this stage as well as the constant μ_2 value maintained at 1000 packets in throughout.

This is the stark contrast to the effect of μ_2 on the response time as seen in Table 5.4. The response time of stage two decreases decreases gradually with increasing BS service rates, μ_2, while the response time at the UAV-RN stage remains [somewhat] constant. This effect is due to more packets leaving stage two per unit time while the service rate of stage one, μ_1, is maintained at 1500 packets per second throughout. Another plausible explanation could be that the razor-thin margin of change of the

MQL values and thus the corresponding response time are being cancelled out by the similar θ_1 and θ_2 values both capped at 0.5 throughout.

To track the effect of buffer length limit, N for the UAVRN stage and L at the BS stage, on queuing performance, we used different capacity limits on both stages of the queue while varying λ_1 at the boundary of critical λ_1 but maintaining the other parameters at the standard values. Table 5.6 shows the effect of N on MQL at both stages while Table 5.7 shows the effect of L on MQL at both stages.

Table 5.6 Effect of UAV-RN buffer length on MQL_{UAVRN} and MQL_{BS}.

MQL_{UAVRN}				MQL_{BS}		
N = 3000						
λ_1	Iter.	Sim	$D\%$	Iter.	Sim	$D\%$
400	0.7444	0.7645	2.629169392	13.6598	13.9929	2.380492964
500	0.9979	0.9991	0.120108097	750	730.7709	2.631344516
600	1.2417	1.2217	1.637063109	1495.998	1484.7462	0.757826489
N = 7500						
400	0.7544	0.7644	1.308215594	13.6768	13.9764	2.14361352
500	0.9988	0.9992	0.040032026	742.83	737.2732	0.753696188
600	1.2445	1.2215	1.882930823	1496.7291	1484.7605	0.806096337
N = 10000						
400	0.7584	0.7645	0.797907129	13.6838	13.9606	1.982722806
500	0.999	0.9994	0.040024014	720.8843	718.8501	0.28297972
600	1.2317	1.2216	0.826784545	1495.998	1484.74	0.758247235

The following parameters were used in tracking the effect of UAV-RN buffer length limit on MQL_{UAVRN} and MQL_{BS}: λ_1 = 500, μ_1 = 2000, λ_2 = 500, μ_2 = 1000, θ_1 = 0.5, θ_2 = 0.5, L = 1500.

The following parameters were used in tracking the effect of BS buffer length limit on MQL_{UAVRN} and MQL_{BS}: λ_1 = 500, μ_1 = 2000, λ_2 = 500, μ_2 = 1000, θ_1 = 0.5, θ_2 = 0.5, N = 1500.

As expected, in both cases investigating the bearing of buffer length limits on mean queue length, the effect of the higher μ_1 value (maintained at 2000 packets per second) meant that the BS stage of the queue governs the stability of the system. Owing to this, the mean queue length at the UAV-RN stage is still observed to be very low in

Table 5.7 Effect of BS buffer length on MQL_{UAVRN} and MQL_{BS}.

MQL_{UAVRN}				MQL_{BS}		
L = 3000						
λ_1	Iter.	Sim	$D\%$	Iter.	Sim	$D\%$
400	0.7444	0.7645	2.629169392	13.6598	13.9929	2.380492964
500	0.9977	0.9987	0.100130169	1439.2315	1443.1317	0.270259464
600	1.2414	1.2214	1.637465204	2995.998	2984.6705	0.379522631
L = 7500						
400	0.7544	0.7644	1.308215594	13.6598	13.9703	2.202971183
500	0.9988	0.9988	0.000000000	3789.2315	3788.7124	0.065001841
600	1.2445	1.2215	1.882930823	7495.998	7484.1805	0.122119763
L = 10000						
400	0.7584	0.7645	0.797907129	13.6598	13.9675	2.202971183
500	0.999	0.9984	0.060096154	4582.2315	4579.2549	0.065001841
600	1.2313	1.2215	0.802292264	9995.998	9983.8058	0.122119763

comparison to that at the BS even after the critical λ_1 has been reached, the MQL at the BS stage is at a value very close to the set buffer length limit and the system is approaching instability. The effect exhibited for the mean queue length is expected to reverberate to the response time as well, similar to the effect of θ_1 and θ_2 showcased in the graphs discussed in this chapter.

5.2.1 The Iterative Solution

Following the results presented in Table 5.1, we can comment on the accuracy of the implemented iterative solution that is the secondary focus of this study. For acceptable ranges of parameters within which the system is stable, we are able obtain performance measures from the analytical model that within the 5% confidence interval of the simulation program [12]. Further proving the correctness of the optimum/standard parameters chosen for our framework.

Forbye, from the above elaborated trend of inferences, we can arrive at the assertion that the analytical solution approach is quite useful in this sense in order to specify the jump point for performance measures of specific configurations. The proposed iterative approach is capable of identifying the highest traffic load a specific configuration

can tolerate as accurately as the simulation while it is computationally significantly more efficient. The fact that the contrasted results consistently diverge past that is further testament to the fulfillment of the objective of the study. We are able to predict the performance measures (discussed above) at this critical λ_1 within the expected error margin of 5% as per the confidence interval of the simulation program [12].

Regarding the iterative solution that is the subject of this study, the following observations can be made about their effect on the analytical model results:

- Given the ***standard*** parameters, more iterations are required to achieve convergence when the sum of θ_1 and θ_2 is further from 1.0 - either below or above 1.0. For instance, the run with θ_1 and θ_2 as 0.5 achieved convergence at determining the critical λ_1 with as low as 5000 iterations while maintaining the results within the desired 5% error margin in line with the confidence interval of the simulation program [12]. In contrast, the run with θ_1 as 0.4 and θ_2 as 0.5 required up to 150000 iterations to achieve the convergence in determining the critical λ_1.

- Despite the general trend exhibited above, it was also evident that at very low lambda values ($\lambda_1 \leq 100$ packets per second), the performance measures converged much faster with as low as 5000 iterations with ϵ as 0.001. In contrast, higher lambda values produced a higher impact of the number of iterations on the results. This is to say that for the same ϵ value, the number of iterations that produced a convergence increased towards the critical λ_1 and decreased away from it. The latter being due to the system approaching instability as the MQL of the second stage increased rapidly to quantities very close to the queue capacity.

- The key advantage of the iterative solution is in its ease of implementation. In this study, we have broken down the approach into composite steps but even prior to this, the premise is much simpler to understand in comparison to other methods such as the product form solution used in [12] by Yaqoob et al.

- One imperative criticism of the iterative solution is identifying the suitable ϵ value to govern the stopping criteria of the iterative model. From the test runs

carried out to obtain the performance measures plotted in the graphs in Figures 5.1 to 5.12 discussed above, the **mode** convergence limit value, ϵ, used was 0.00000001 resulting in a convergence within the 5% confidence interval of the simulation program [12].

At this point, we can compare the temporal computational performance of the analytical solution against the custom simulation used for validating the model. Table 5.5 contrasts the CPU run-times of the iterative analytical model with that of the simulation program. The computer architectural specifications of the machine used for the analytical solution were as follows: Processor - 2.7 GHz Quad-Core Intel Core i7, Memory (RAM) - 16 GB 2133 MHz LPDDR3 (Low-Power Double Data Rate 3). In this run of tests comprising the standard parameters, the proposed iterative solution consistently outperforms the simulation program. The MQL values in the analytical solution converged within 2 iterations, given ϵ as 0.001. Further affirming the validity of this set of values as our standard operating parameters. Owing to this, the above mentioned trends could prove a useful blueprint seeing as a pattern does form depending on the nature of the parameters in question. Sets of values that experience quick convergence require a much higher ϵ value. For instance, taking θ_1 and θ_2 as 0.5 i.e., $\theta_1 + \theta_2 = 1.0$, we are able to get convergences with as low as 5000 iterations and the results are within acceptable error margins governed by the confidence interval of the simulation program [12].

CHAPTER 6

LIMITATIONS AND FUTURE WORK

In this chapter, we explicitly discuss the shortcomings of the proposed solution and their implications as well as possible future research questions that may arise or gaps that may be exploited due to this study.

6.1 Limitations of this study

Although we have heavily heralded the model presented in this study, it would be judicious to point out the limitations of the solution as well. Indeed, some of the limitations initiate lines of questioning that invoke future works of research, further emphasizing the importance of this section.

The limitations we can point out include:

- The arbitrary nature of the limit of convergence, ϵ. In this study, a lot of trial and error is employed in finding the most appropriate ϵ value that governs the number of iterations. This can be very time consuming especially in the testing phase. It would be of much benefit if a more intuitive approach were adopted to at least find the best [range of] ϵ value(s).

- The analytical model still spots a huge error discrepancy in the results obtained and is extremely sensitive to system instability. In the graphs provided in Chapter 5.2, the discrepancy between the analytical and simulation results immediately exceeds the 5% confidence interval after the critical λ_1. Even though this does not tamper with the correctness of the results per se, it leaves very little wiggle room for the model.

- The initial conditions under which the state probabilities, $P_{i,j}$'s, to kick off the

model are calculated could be improved further to curb the effect of the above limitations as well as reduce the number of iterations needed for convergence to be achieved.

6.2 Future work

Despite the comprehensive nature of the model we have proposed in this study, there remain several issues that can still be addressed in the research:

- Comprehensive energy consumption models for UAV-assisted networking solutions can still be improved. Specifically, frameworks that involve the use of UAVs solely as relay nodes and not as hovering base stations.
- Line-of-sight (LoS) analysis and its effect on queuing performance of UAV-RNs in disaster recovery can be incorporated into the analytical solution. Additionally, subsequent remedies for LoS issues can be adapted for future analytical solutions presented for UAV-RNs being utilised in this context.
- Concerning the queuing model, we could further incorporate breakdowns and repairs of the UV-RNs and BSs to stress-test the model.
- It would also be interesting to explore the effect of the rapid mobility of the UAV-RNs on the queuing performance measures in the framework.
- Considering the example of a densely populated localised disaster area such as a football field, the need to conceptually divide the cell into micro-cells would arise to avoid overloading a single UAV-RN providing coverage to stranded UEs. This would call for multiple UAV-RNs to deployed in the same disaster space. It would be interesting to proffer an analytical model that incorporates inter-UAVRN communication in such a context.

CHAPTER 7

CONCLUSION

As per the projected contributions of this study outlined in Section 1.2, we have considered a rapidly mobile relaying scheme for wireless networks during disaster recovery for performance evaluation with the intention of providing an analytical solution to the queuing in UAV-RN/UAV-based wireless solutions in this context.

The scheme under study has been modelled using a two-stage tandem queuing system and used to investigate the effect of varying system parameters particularly at the mobile relay node - arrival rates, service rates, relaying and feedback probabilities - on key performance measures namely mean queue length, throughput and response time.

In addition, with a novel augmented approach to generating the initial conditions, an iterative method has been explored to provide an analytical solution for the proposed queuing system with very large queue sizes to circumvent the state explosion problem that is characteristic of the generic matrix solution. This is in a bid to define the ideal parameters under which the system would operate while maintaining its stability.

As has been asserted in the preceding section (5.2), we have been successful in identifying [what we have termed as] the **critical** primary UAV-RN arrival rate, λ_1 i.e., the optimum primary arrival rate of packets at the UAV-RN for various relaying (θ_1) and feedback probabilities (θ_2).

Subsequently, the results from the proposed analytical model contrasted against those from a custom simulation program. This critical λ_1 has been identified within the expected confidence interval of the simulation.

With reference to the proposed iterative solution, we have identified that it allows us to carry out performance analysis for very large queue sizes. In our case, the standard

size assumed in the iterative solution (1500 x 1500) is ten times the maximum queue size computationally permissible in the system of simultaneous equations solution (150 x 150). Additionally, for the standard set of parameters discussed in Section 5.1, the proposed iterative solution provides a faster solution than the simulation program as in Table 5.5. Conversely, we have deliberated on the shortcoming of the iterative solution citing the difficulty in identifying the most appropriate value for the limit of convergence, ϵ, and gone ahead to point out that seeking an improved starting point for our initial state probabilities, $P_{i,j}$'s would aid in this.

Furthermore, we have explored future research questions that could arise from this study and the foundation that the information we have put forward would provide in any such case.

Bibliography

[1] Nan Zhao, Weidang Lu, Min Sheng, Yunfei Chen, Jie Tang, F. Richard Yu, and Kai-Kit Wong. Uav-assisted emergency networks in disasters. *IEEE Wireless Communications, INTEGRATING UAVS INTO 5G AND BEYOND*, February 2019.

[2] Mohammad Mozaffari, Walid Saad, Mehdi Bennis, and M{'erouane Debbah. Efficient deployment of multiple unmanned aerial vehicles for optimal wireless coverage. *IEEE COMMUNICATIONS LETTERS*, 20(8), August 2016.

[3] Enver Ever, Eser Gemikonakli, Huan X. Nguyen, Fadi Al-Turjman, and Adnan Yazici. Performance evaluation of hybrid disaster recovery framework with d2d communications. *Computer Communications*, 2020.

[4] M. Erdelj and E. Natalizio. Uav-assisted disaster management: Applications and open issues. pages 1–5, Feb. 2016.

[5] E. Christy and et. al. Optimum uav flying path for device-to- device communications in disaster area. page 318–22, May 2017.

[6] Y. Chen and et. al. Multiple uavs as relays: Multi-hop single link versus multiple dual-hop links. *IEEE Trans. Wireless Commun.*, 17(9):6348–6359, Sept. 2018.

[7] Safa'a S. Saleh, Tamer F. Mabrouk, and Rana A. Tarabish. An improved energy-efficient head election protocol for clustering techniques of wireless sensor network (june 2020). *Egyptian Informatics Journal*, pages 439–445, 2021.

[8] Bander Alzahrani, Omar Sami Oubbati, Ahmed Barnawi, Mohammed Atiquzzaman, and Daniyal Alghazzawi. Uav assistance paradigm: State-of-the-art in applications and challenges. *Journal of Network and Computer Applications*, 166(102706), September 2020.

[9] Fenyu Jiang and Chris Phillips. High throughput data relay in uav wireless networks. *Future Internet*, 12:193, 2020.

[10] Yixin He, Daosen Zhai, Dawei Wang, Xiao Tang, and Ruonan Zhang. A relay selection protocol for uav-assisted vanets. *Applied Sciences*, 10(8762), 2020.

[11] Nabhendra Bisnik and Abouzeid Alhussein. Queuing network models for delay analysis of multihop wireless ad hoc networks. *Ad Hoc Networks*, 7:79–97, 08 2009.

[12] Mahnoor Yaqoob, Enver Ever, and Orhan Gemikonakli. Modelling heterogeneous future wireless cellular networks: An analytical study for interaction of 5g femtocells and macro-cells. *Future Generation Computer Systems*, 114:82–95, 2020.

[13] Orhan Gemikonakli, Enver Ever, and Altan Kocyigit. Approximate solution for two stage open networks with markov-modulated queues minimizing the state space explosion problem. *Journal of Computational and Applied Mathematics*, 223:519–533, 2007.

[14] Xu Jiang, Mi Sheng, Nan Zhao, Chengwen Xing, Weidang Lu, and Xianbin Wang. Green uav communications for 6g: A survey. *Chinese Journal of Aeronautics*, April 2021.

[15] Gurkan Tuna, Tarik Mumcu, and Kayhan Gulez. Design strategies of unmanned aerial vehicle-aided communication for disaster recovery. pages 115–119, 12 2012.

[16] Arvind Merwaday and Ismail Guvenc. Uav assisted heterogeneous networks for public safety communications. In *2015 IEEE Wireless Communications and Networking Conference Workshops (WCNCW)*, pages 329–334, 2015.

[17] Jó Ueyama, Heitor Freitas, Bruno Faiçal, Geraldo Filho, Pedro Fini, Gustavo Pessin, Pedro Gomes, and Leandro Villas. Exploiting the use of unmanned aerial vehicles to provide resilience in wireless sensor networks. *IEEE Communications Magazine*, 52, 12 2014.

[18] William H. Robinson and Adrian P. Lauf. Aerial manets: Developing a resilient and efficient platform for search and rescue applications. *J. Commun.*, 8:216–224, 2013.

[19] Paul Bupe, Rami Haddad, and Fernando Rios-Gutierrez. Relief and emergency communication network based on an autonomous decentralized uav clustering network. In *SoutheastCon 2015*, pages 1–8, 2015.

[20] Marco Di Felice, Angelo Trotta, Luca Bedogni, Kaushik R. Chowdhury, and Luciano Bononi. Self-organizing aerial mesh networks for emergency communication. *2014 IEEE 25th Annual International Symposium on Personal, Indoor, and Mobile Radio Communication (PIMRC)*, pages 1631–1636, 2014.

[21] Panagiotis Vamvakas, Eirini Eleni Tsiropoulou, and Symeon Papavassiliou. On the prospect of uav-assisted communications paradigm in public safety networks. In *IEEE INFOCOM 2019 - IEEE Conference on Computer Communications Workshops (INFOCOM WKSHPS)*, pages 762–767, 2019.

[22] Yong Zeng, Rui Zhang, and Teng Joon Lim. Wireless communications with unmanned aerial vehicles: Opportunities and challenges. 11 Feb 2016.

[23] Saul I. Gass and Michael C. Fu. Encyclopedia of operations research and management science: Kendall's notation. `https://link.springer.com/referenceworkentry/10.1007/978-1-4419-1153-7_200360`, 2016. Accessed: 2022-05-19.

[24] Enver Ever, Purav Shah, Leonardo Mostarda, Fredrick Omondi, and Orhan Gemikonakli. On the performance, availability and energy consumption modelling of clustered iot systems. *Computing*, 101:1935–1970, 2019.

[25] Hasini Viranga Abeywickrama, Beeshanga Abewardana Jayawickrama, Ying He, and Eryk Dutkiewicz. On the performance, availability and energy consumption modelling of clustered iot systems. *IEEE Access*, 6, 2018.

[26] Mohammad Mozaffari, Walid Saad, Mehdi Bennis, Young-Han Nam, and Merouane Debbah. A tutorial on uavs for wireless networks: Applications, challenges, and open problems. 17 Mar 2019.

[27] TechTarget. Network Packet. https://www.techtarget.com/searchnetworking/definition/packet#:~:text=Typically%2C%20a%20packet%20holds%201%2C000,internet%20address%20of%20the%20destination, July 2021. Accessed: 2022-04-23.

[28] LIFEWIRE: Tech For Humans. 5G: Everything You Need to Know. https://www.lifewire.com/5g-wireless-4155905#:~:text=5G%20Supports%20Lots%20of%20Devices,internet%20at%20the%20same%20time, June 18, 2021. Accessed: 2022-06-19.

[29] Rui Han, Jiaxing Wang, Lin Bai, Jianwei Liu, and Jinho Choi. Age of information and performance analysis for uav-aided iot systems. *IEEE Internet of Things*, (2327-4642), 2020.

[30] Cisco. Cisco Mobile Wireless Home Agent Release 5.1 for Cisco IOS Release 12.4(22)YD1. https://www.cisco.com/c/en/us/td/docs/ios/12_4/12_4x/12_4_22yd1/feature_guide/ha_5_1_feat/ha_over.html, 2019. Accessed: 2022-05-30.

[31] Yonal Kirsal, Enver Ever, Altan Kocyigit, Orhan Gemikonakli, and Glenford Mapp. Modelling and analysis of vertical handover in highly mobile environments. *J Supercomputers*, 71, 2015.

[32] Saied M. Abd El-atty, Z. M. Gharsseldien, and Konstantinos A. Lizos. Predictive reservation for handover optimization in two-tier heterogeneous cellular networks. *Wireless Personal Communications*, 98:1637–1661, 2018.

[33] Yonal Kirsal, Enver Ever, Altan Kocyigit, Orhan Gemikonakli, and Glenford Mapp. A generic analytical modelling approach for performance evaluation of the handover schemes in heterogeneous environments. *Wireless Personal Communications*, 79:1247–1276, July 2014.

[34] Droneblog. How Far Can a Drone Fly (from the Controller)? https://www.droneblog.com/how-far-can-a-drone-fly-from-the-controller/, 2022. Accessed: 2022-05-19.

[35] Network encyclopedia: Cell in wireless communication. https://networkencyclopedia.com/cell-in-wireless-communication/, 2022. Accessed: 2022-05-30.

[36] Birsen Donmez, Carl Nehme, and Mary L. Cummings. Modeling workload impact in multiple unmanned vehicle supervisory control. *IEEE Transactions on*

Systems, Man, and Cybernetics-Part A: Systems and Humans, 40:1180–1190, 2010.

[37] Jerry Banks, John S. II Carson, Barry L. Nelson, and David M. Nicol. *Discrete-Event System Simulation*. Prentice Hall - PEARSON EDUCATION, India, 4 edition, 2005.

[38] Saied M. Abd El-atty and Zakaria M. Gharsseldien. Performance analysis of an advanced heterogeneous mobile network architecture with multiple small cell layers. *Wireless Networks*, 23:1169–1190, 2017.

[39] Prabhu Chandhar and Erik G. Larsson. Massive mimo for connectivity with drones: Case studies and future directions. *IEEE*, 2019.

[40] Specifications for the intel® aero ready to fly drone. `https://www.intel.com/content/www/us/en/support/articles/000023272/drones/development-drones.html`, February 2019. Accessed: 2022-09-1.

[41] Stanley C. F. Chan, K. M. Chan, Ke Liu, and Jack Y. B. Lee. On queue length and link buffer size estimation in 3g/4g mobile data networks. *IEEE Transactions on Mobile Computing*, 13:1298–1311, 2014.

APPENDIX A

MISCELLANEOUS

Note

Equation labels follow the format Chapternumber+Equationnumber e.g ., Equation 410 tracks Chapter 4 Equation 10.

Parameters for analytical modeling

Standard system parameters: UAVRN arrival rate = 500 packets/second , UAVRN service rate = 2000 packets/second, Relaying probability = 0.5, BS arrival rate = 500 packets/second, BS service rate = 1000 packets/second, Feedback probability = 0.5.

NB: During the test runs for analytical model, the quantity whose effect is being monitored (relaying probability, feedback probability and UAVRN service rate) is varied while the rest are kept constant at the above given standard values. When monitoring the effect of BS service rate, all other quantities are kept constant but UAVRN service rate is held at 1000 packets /second.

Percentage discrepancy ranges for analytical modeling results

NB: All percentage discrepancies are below 5.0000

Effect of relaying probability:

Effect on UAVRN MQL; 0.1201 to 4.0313

Effect on BS MQL; 0.4504 to 4.0212

Effect on UAVRN Throughput; 0.0184 to 3.7826

Effect on BS Throughput; 0.0167 to 1.1618

Effect on UAVRN RT; 0.1017 to 2.8014
Effect on BS RT; 0.2650 to 4.8455

Effect of feedback probability:

Effect on UAVRN MQL; 0.0600 to 3.7391
Effect on BS MQL; 0.2482 to 3.0768

Effect on UAVRN Throughput; 0.0025 to 4.8068
Effect on BS Throughput; 0.0166 to 0.8610

Effect on UAVRN RT; 0.0681 to 4.6566
Effect on BS RT; 0.2650 to 3.0941

Effect of UAVRN service rate:

Effect on UAVRN MQL; 0.01689 to 3.8252
Effect on BS MQL; 0.37904 to 4.5442

Effect on UAVRN RT; 0.0814 to 3.8215
Effect on BS RT; 0.3960 to 4.5298

Effect of BS service rate:

Effect on UAVRN MQL; 0.0164 to 2.4910
Effect on BS MQL; 0.3790 to 3.7386

Effect on UAVRN RT; 0.19358 to 2.5060
Effect on BS RT; 0.03164 to 0.09238

System parameters for monitoring the effect of buffer length on MQL

Effect of UAVRN buffer length:

System parameters; UAVRN arrival rate = 500 packets/second, UAVRN service rate = 2000 packets/second, BS arrival rate = 500 packets/second, BS service rate = 1000 packets/second, relaying probability = 0.5, feedback probability = 0.5, BS buffer length, L = 1500.

Effect of BS buffer length:

System parameters; UAVRN arrival rate = 500 packets/second, UAVRN service rate = 2000 packets/second, BS arrival rate = 500 packets/second, BS service rate = 1000 packets/second, relaying probability = 0.5, feedback probability = 0.5, UAVRN buffer length, N = 1500.

NB: The discrepancy ranges for the effect of buffer length on mean queue length are visible from the tables in the text.

TEZ İZİN FORMU / THESIS PERMISSION FORM

PROGRAM / PROGRAM

Sürdürülebilir Çevre ve Enerji Sistemleri / Sustainable Environment and Energy Systems ☐

Siyaset Bilimi ve Uluslararası İlişkiler / Political Science and International Relations ☐

İngilizce Öğretmenliği / English Language Teaching ☐

Elektrik Elektronik Mühendisliği / Electrical and Electronics Engineering ☐

Bilgisayar Mühendisliği / Computer Engineering ☒

Makina Mühendisliği / Mechanical Engineering ☐

YAZARIN / AUTHOR

Soyadı / Surname : Owilla

Adı / Name : Eugene

Programı / Program : Computer Engineering

TEZİN ADI / TITLE OF THE THESIS (**İngilizce** / English) : AN ANALYTICAL APPROACH FOR MODELLING UNMANNED AERIAL VEHICLES AND BASE STATION INTERACTION FOR DISASTER RECOVERY SCENARIOS

TEZİN TÜRÜ / DEGREE**:** **Yüksek Lisans** / Master ☒ **Doktora** / PhD ☐

1. **Tezin tamamı dünya çapında erişime açılacaktır. /** Release the entire work immediately for access worldwide. ☐

2. **Tez iki yıl süreyle erişime kapalı olacaktır.** / Secure the entire work for patent and/or proprietary purposes for a period of **two years. *** ☐

3. **Tez altı ay süreyle erişime kapalı olacaktır.** / Secure the entire work for period of **six months**. * ☒

Yazarın imzası / Author Signature ..... **Tarih** / Date 29.08.2022

Tez Danışmanı / Thesis Advisor Full Name: Assoc. Prof. Dr. Enver Ever

Tez Danışmanı İmzası / Thesis Advisor Signature: .....

Eş Danışmanı / Co-Advisor Full Name: NA

Eş Danışmanı İmzası / Co-Advisor Signature: NA

Program Koordinatörü / Program Coordinator Full Name: Assoc. Prof. Dr. Enver Ever

Program Koordinatörü İmzası / Program Coordinator Signature: .....